PART I - DIFFUSION OF Si IN Al AND SOLID PHASE GROWTH OF EPITAXIAL Si STRUCTURES IN Al

PART II - INVESTIGATION ON THE Si-Au INTERFACE EFFECTS AND ON THE PHASE DIAGRAM OF Si-Au-Cu

Thesis by

Haluk Sankur

In Partial Fulfillment of the Requirements

For the Degree of

Doctor of Philosophy

California Institute of Technology

Pasadena, California

1975

(Submitted May 14, 1975)

To my wife, Vega

ACKNOWLEDGMENTS

I am greatly indebted to Professor J. O. McCaldin for his assistance, guidance and valuable insight. My association with him has been intellectually stimulating, interesting and rewarding.

I am also indebted to Dr. J. W. Mayer for his encouragement, to Dr. M-A. Nicolet for the use of vacuum evaporation and associated equipment, to Professor P. Duwez for the use of X-ray diffractometer and its associated equipment. Special thanks to R. Cunningham of North American Rockwell and A. Chodos of Caltech for the microprobe work, to J. Devoney and K. Evans of JPL for SEM work, to J. Wysocki for his services in the preparation of the alloys, to R. Gorris for his valuable advice and aid in technical matters.

I extend my gratitude to JPL, NASA for the use of SEM and metallographic facilities, as well as for financial support; to the Kodak Company, Office of Naval Research, and E. C. Anthony fellowship for financial assistance; and to Chemical Engineering department and student center for extending the use of tools and machine shop facilities throughout my graduate study.

Finally, I thank my wife, Vega, for her patience, affectionate encouragement and exchange of valuable ideas through my graduate years.

ABSTRACT

PART I

Reactions between solid metal films and semiconductors are important in the reliability, operation of semiconductor devices and growth of semiconductor structures in solid state. In this work diffusion and precipitation of Si in Al films and growth of Si epitaxial structures in solid Al have been studied.

Diffusivity and solubility of Si in Al films of an integrated circuit structure have been investigated by means of electron microprobe analysis at temperatures between 360^{o}C and 560^{o}C. The Si solubility was found to be in essential agreement with values reported in the literature for bulk Al. The Si diffusivity was found to be enhanced with respect to bulk values and the activation energy for diffusion reduced by 42% from bulk value to 0.8 eV. The enhanced diffusivity and reduced activation energy are due to the presence of a large number of structural defects--mainly dislocations--in the evaporated Al film.

The thin Al films were also analyzed for the ultimate location of Si precipitation with the electron microprobe. Si in solution in Al becomes supersaturated and precipitates upon cooling from the dissolution temperature. Si in Al considerably less than a diffusion length from the substrate Si was found to regrow there. Elsewhere Si formed precipitates, preferentially near the free surface of the Al film.

In view of the results of the precipitation experiments, investigation of the growth of Si epitaxial structures in solid Al onto crystal

Si substrates was performed by means of scanning electron microscopy. A variety of growth structures, such as mesas, faceted structures, thin vertical membranes, large plateaus were observed. The morphology of these structures depended on the amount of Si deposited in the Al film, annealing conditions, stresses in the metal film, crystalline orientation of the substrate surface.

Preferential growth was observed to occur at reentrant corners and small diameter oxide cuts. The probable cause for such preferential growth was indicated in pressure experiments which showed that regions in the solid Al under relatively less compression are favored locations for growth.

PART II

Interface conditions between a metal and a metal or semiconductor are known to affect solid state reactions there. In the present work dissolution reaction of crystalline and amorphous Si into evaporated Au films was studied with electron microprobe and scanning electron microscopy. The dissolution pattern was found to be nonuniform along the plane of the surface and dependent on the crystalline orientation of the Si substrate. The latter behavior was changed upon evaporation of a thin Pd layer between Au and Si, which greatly facilitated the dissolution reaction.

Investigation of Si dissolution in Au by electron microprobe analysis also indicated that Si solubility was below the sensitivity of this analysis technique. A study of Si-Au-Cu ternary solid solution

was undertaken in view of the more extensive solubility of Si in Cu compared to that in Au. The analysis, which was performed by powder X-ray diffraction and micrography, indicated that a continuous ternary solid solution existed through most of the Cu-Au solubility range, and that it was in equilibrium with a phase, with cubic lattice structures. The solubility of Si deviated from the linear interpolation of binary solubilities and from a monotonically decreasing behavior going from Cu-rich toward Au-rich corner of the diagram.

Parts of this thesis have been previously published under the following titles:

Diffusivity and solubility of Si in the Al metallization of integrated circuits. J. O. McCaldin and H. Sankur, Appl. Phys. Lett. 19, 524 (1971).

Precipitation of Si from the Al metallization of integrated circuits. J. O. McCaldin and H. Sankur, Appl. Phys. Lett. 20, 171 (1972).

Solid-phase epitaxial growth of Si mesas from Al metallization. H. Sankur, J. O. McCaldin and J. Devaney, Appl. Phys. Lett. 22, 64 (1973).

Interface effects in the dissolution of silicon into thin gold films. H. Sankur and J. O. McCaldin, J. Electrochem. Soc. 122, 565 (1975).

Phase boundary of ternary solid solution in Cu-Au-Si. H. Sankur, to be published.

TABLE OF CONTENTS

PART I

DIFFUSION OF Si IN Al AND SOLID PHASE GROWTH OF EPITAXIAL Si STRUCTURES IN Al

I. INTRODUCTION

A. General

The general trend in the semiconductor electronic device industry has been the elimination of the reliability problems by improvement of techniques and materials and the reduction in device size, mainly to achieve a lower unit cost. A poorly understood region of the devices in the former respect was the metal semiconductor contacts. The present investigation of metal-semiconductor interfacial phenomena led not only to a more complete physical understanding of device contacts, but also to a novel and simple technique of fabricating active parts of devices at arbitrarily small dimensions in solid state.

Connection to the active parts of semiconductor devices and interconnections between various active or passive devices in an integrated circuit are made with a vapor deposited and photolithographically delineated metallization scheme. Aluminum films are the most widely used metallization system in the discrete devices and integrated circuits made with Si and with the present technology. This fact is due to the low cost, good conductivity of Al, simplicity in deposition and photolithographic patterning and properties of Al such as strong adherence to both Si and SiO_2 substrate, relative ductility and resistance to oxidation (for example, [1]). However, some reliability aspects of Al metallizations, among which there were the contact problems [2-6] as explained below, led the industry to consider other metals or compounds for interconnections, in spite of many advantages of Al.

It was known that Al dissolved up to 1.4% Si [7] and that partial saturation of Al metallization with Si--dissolution of Si at contact cuts and transport of Si along metal lines--occurred rapidly enough to take place during such thermal excursions in the manufacturing as contact "forming", passivation glass fritting, package sealing. A problematical aspect of the above mentioned facts was that dissolution pattern at the contact cuts was uneven and such as to produce pits at the contact periphery, that is, Si-SiO_2 boundary (Fig. 1). The pitting led to shorts between thin planar diffused layers, or at best, caused excess leakage currents and soft breakdown characteristic of junctions. This problem is eliminated in the present technology by incorporating Si in the Al films, in order to suppress the Si dissolution.

A different reliability aspect becomes important when the dissolved Si precipitates and grows back in crystalline form on the original Si surface upon cooling the device from high temperatures during treatment. The Si, dissolved in Al to its equilibrium solid solubility, becomes supersaturated and segregates into a Si rich phase when the temperature is decreased [8]. Under suitable conditions, the precipitation can occur as epitaxial regrowth on a Si substrate. The regrown structures incorporate Al as dopant, hence become p-type Si [9]. If the substrate or the region at the contact cut is n-type Si, these structures will then form a p-n junction instead of an intended ohmic contact or Schottky diode, when the surface area coverage of these is complete; a decrease of the useful contact area or formation of a noisy junction will result if the coverage is partial. Both of these effects are undesirable from device reliability point of view [10,11].

Fig. 1

SEM picture of the Si surface after extensive Si dissolution in Al has taken place. Note the faceting of some pits that reflect crystalline symmetry of the substrate, and different rates of the dissolution of various crystalline planes. The lower SEM picture is a contact cut in an integrated circuit analyzed by the author in JPL's failure analysis lab. Al has been removed by etching.

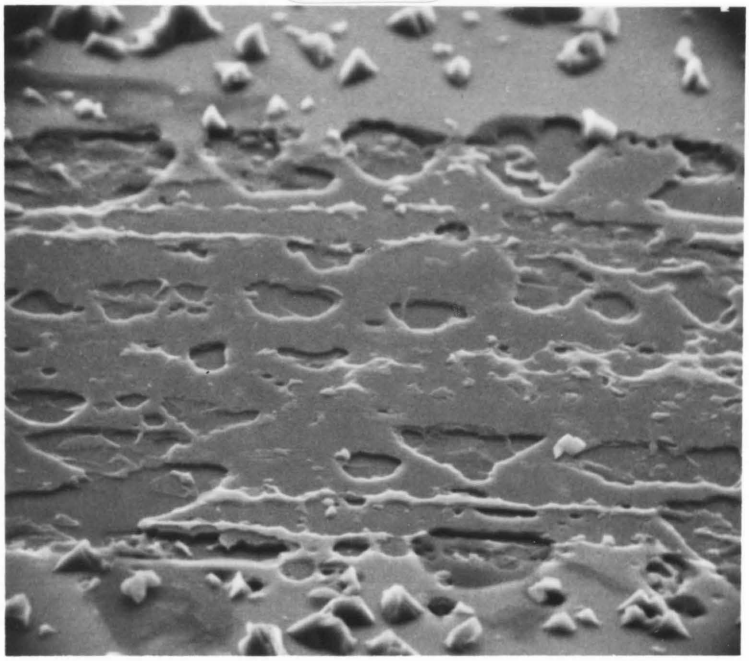

10 μ

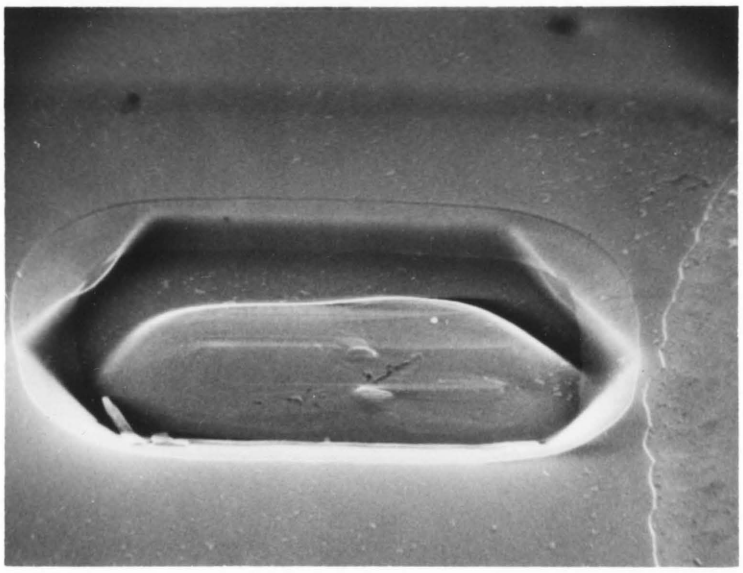

On the other hand, the regrowth of epitaxial layers in solid state can be advantageously used to produce layers of very small dimensions in active parts of devices. In general, interdiffusion and reactions in metal-semiconductor layers have been shown to be important in the operation, performance and failure of semiconductor devices, as well as usable in their fabrication.

The diffusion of semiconductor elements has been shown to occur at low subeutectic temperatures for Ge-Al [12,13], Si-Al [14], Si-Ag and Ge-Ag [15], Si-Au [16-18], which are all simple eutectic systems. In the first three systems, semiconductor elements were also observed to crystallize within the solvent metal matrix at about 7/10 of their respective eutectic temperatures [19-23]. Solid state reactions have been studied for compound forming systems such as Hf-Si [24], Pt-Si [18], V-Si [25], Nb-Si [26], and Ti-Si [26,37], Cr-Si, Mo-Si [27], Pd-Si [27-29], Ti-Al-Si [30], and with metal-compound semiconductors such as GaAs-Pt [31], GaAs-Au [31,32], GaAs-Au-Ge [32,33]. The above mentioned crystallization of semiconductors in contact with metals had been previously observed for CdS-Ag and a number of other metals [34], ZnS-Cu [35]. The epitaxial growth of Si or Ge was observed to occur on the substrate surface for Si-Al [9], Ge-Al [36,37], Si-Ni through Ni_2Si [38], Pd-Si through Pd_2Si [39].

The growth of epitaxial semiconductor structures in solid state should offer distinct advantages for the fabrication of devices. A greater dimensional control is achieved, mainly due to diffusion limited nature and slow rate of growth, and also due to absence of

surface tension as in liquid phase epi-growth. Another advantage of this low temperature process should be the reduced introduction of unwanted impurities such as fast diffusing impurities, impurities that form midgap states and are deleterious to carrier lifetime sensitive devices, structural defects such as vacancies, stacking faults, defects arising out of plastic flow due to thermal stresses such as dislocation loops and slip lines. Secondary advantages are the elimination of such effects as out-diffusion of previously implanted or diffused impurities, and of chemical decomposition that takes place in high temperature treatment of devices during conventional manufacturing. However, considerably more investigation should be done before a realistic assessment of its advantages can be made.

The possibility of fabricating useful electrical devices was demonstrated in Si-Al [9]. Investigations on Ge-Al systems had also indicated the possibility of making transistors [40], hole injecting contacts for diodes, and double injection diodes [41], blocking contacts on nuclear particle detectors [42].

B. Diffusion of Si in Al Thin Films

Diffusion and solubility of Si in vapor deposited Al films has been studied in the present investigation using electron microprobe analysis. The information on the kinetics of transport in solid state in the Si-Al system is important in predicting dissolution reaction and controlling growth of crystalline structures.

The electron microprobe is a chemical analysis instrument that provides a means of studying the local composition of heterogeneous

materials. This is done by irradiating the sample with an energetic electron beam, focused to 1μ diameter or less, to generate the characteristic X-rays of the elements. The focusing of the probing beam allows detection of masses as small as 10^{-15}gm. The X-rays are Bragg diffracted by means of a crystal, and detected by a proportional or solid state counter.

Si was allowed to diffuse along Al thin films (Fig. 2) in a structure similar to conventional integrated circuit metallizations: Al was in contact with Si along restricted areas, which became a source of Si, but otherwise rested on a SiO_2 layer. The concentration profile of Si along the diffusion path was analyzed with an electron microprobe. Diffusivity values for the evaporated film were found to be substantially enhanced compared with the values for bulk or wrought Al; whereas activation energy for diffusion was found to be 58% of the bulk value, in good agreement with other investigators' results [43].

C. Precipitation of Si from Al Metallizations and Growth of Si Epitaxial Structures

The precipitation sites of Si dissolved in Al films was investigated by means of the electron microprobe analysis in structures similar to those used for diffusion studies. Dissolved Si less than a diffusion length was found to regrow on the original Si substrate upon slow cooling. Si in solution, away from crystalline Si substrate, formed precipitate lumps near the free surface of the Al film. Most of the Si was retained in solution upon quenching, which corresponded to cooling of the specimen from

Fig. 2

Cross sectional view of the specimens used in diffusion experiments. Note that vertical dimensions are not to scale. Arrows suggest the predominantly horizontal diffusion path, typically 200-300μ long.

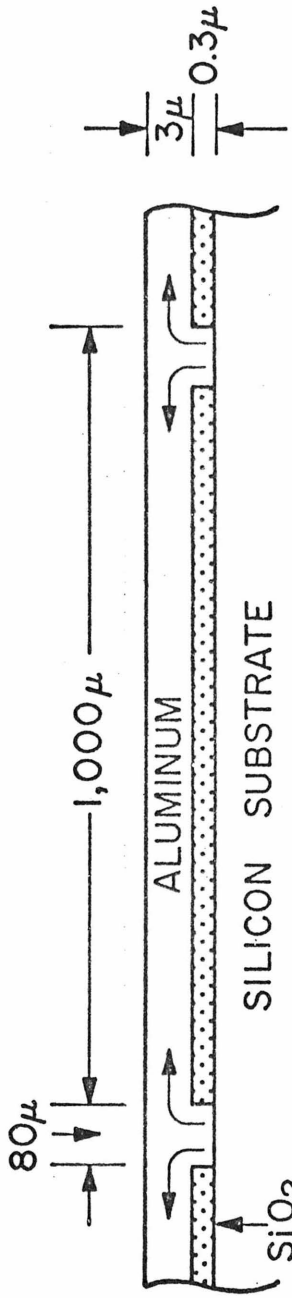
3μ
0.3μ
1,000μ
80μ
ALUMINUM
SILICON SUBSTRATE
SiO2

annealing temperature to room temperature in 1-2 sec.

The growth structures were difficult to study in the aforementioned specimens. The structures were small due to limited quantity of Si in solution available for growth and were difficult to identify unambiguously within the dissolution pattern of the substrate. Therefore an additional source for Si was provided by evaporation of an amorphous Si layer in Al. The greater free energy of the amorphous state over that of the crystalline Si provided the driving force for dissolution, transport of the evaporated layer and growth of epitaxial structures.

Scanning electron microscope investigations showed that the growth structures were in the form of mesa shaped islands, with a preference to grow at reentrant corners like Si-SiO_2 boundaries. These structures filled small sized cuts in the oxide completely. The morphology of these structures could be changed with temperature treatment and amount of Si deposited in Al.

D. Role of Pressure in the Growth of Si Structures

The preference of Si to grow at reentrant corners where the thermal stresses during cooling are such as to produce tension in the Al films indicated that precipitation of Si from Al caused relaxation of stress. An experiment designed to emphasize the factor of mechanical stress indicated that Si is preferentially dissolved in locations where stresses are compressive and grows in adjacent locations that are not stressed.

Electrical characterization of the above mentioned growth structures indicated that they were p-type and that they formed a rectifying junction with the underlying n-type substrate.

II. DIFFUSIVITY AND SOLUBILITY OF Si IN Al THIN FILMS

A. Sample Preparation and Analysis

Samples were prepared with 1-10Ω-cm Si wafers, the surfaces of which were perpendicular to (111) axis. One side of the wafers were polished with SiC and etched in $1HF:1HNO_3:1CH_3COOH$ to remove the damaged layer. A thermal oxide 3000Å thick, was grown on the wafer in wet N_2, a pattern of cuts etched in by photolithography as shown in Fig. 2 in cross section. The cuts in the oxide were in the form of 80μ wide channels which acted as Si sources for diffusion. The separation between channels was ∿ 1000μ, long enough to give adequate diffusion length to Si and to keep the concentration profile simple to analyze by preventing the interaction of Si sources. The wafers were dipped in dilute HF, rinsed with deionized water, dried, loaded into the evaporator. An Al film, 3μ in thickness, was evaporated from a W filament at a pressure of 10^{-5}-10^{-6}torr, onto the room temperature substrates.

The specimens were thereafter subjected to isothermal treatment in a preheated quartz lined tube furnace, through which dry Ar was flowing. The specimen was inserted in the furnace by placing it onto a preheated quartz platform and removed with the same in 1-2 sec and dropped onto a cool asbestos surface.

An alumel-chromel thermocouple calibrated at the melting point of Zn, and sheathed in a 3 mm quartz tube, was used to measure the temperature. The thermocouple, hence the specimen, rose to the steady

state temperature within 2 min. The shortest annealing time was therefore arranged so as to prevent uncertainties in the effective annealing times.

Bulk diffusion studies were performed on specimens prepared by pressing 99.9999% purity, 0.6 mm Al wire against a Si wafer and heat treating this structure in a dry Ar atmosphere. Subsequently, a 12^{o} bevel section of Si-Al interface was made by lapping the structure in alumina powder.

A thin film specimen processed identically except for heat treatment served as control.

The Si concentration was measured with an ARL electron microprobe. The beam voltage was 10^{4}V, the beam current 10^{-7}A, and the focused beam measured 5μ in diameter. Counts were taken at typically 10-15μ intervals for 100 sec along a path perpendicular to the oxide cut boundary, with the detector tuned to $Si_{K\alpha}$. The beam voltage and the Al film thickness were such that the electron beam sampled the upper half of the film and therefore did not excite the substrate Si. The background level allowed us to measure Si down to .01% concentration.

The concentration profile plotted on semilog paper was compared with complementary error function plots where the diffusivity term in the argument of the function was varied until a good fit was obtained. Often error functions with two different D values, differing by as much as 20%, were necessary to obtain fit on different parts of the experimental curve (Fig. 3).

Fig. 3

A typical concentration profile of Si in evaporated Al, measured with microprobe. Diffusion temperature was 446^{o}C and diffusion time 40 min. The continuous curve is a fit to low concentration values, whereas the dashed curve is a fit to values closer to the origin.

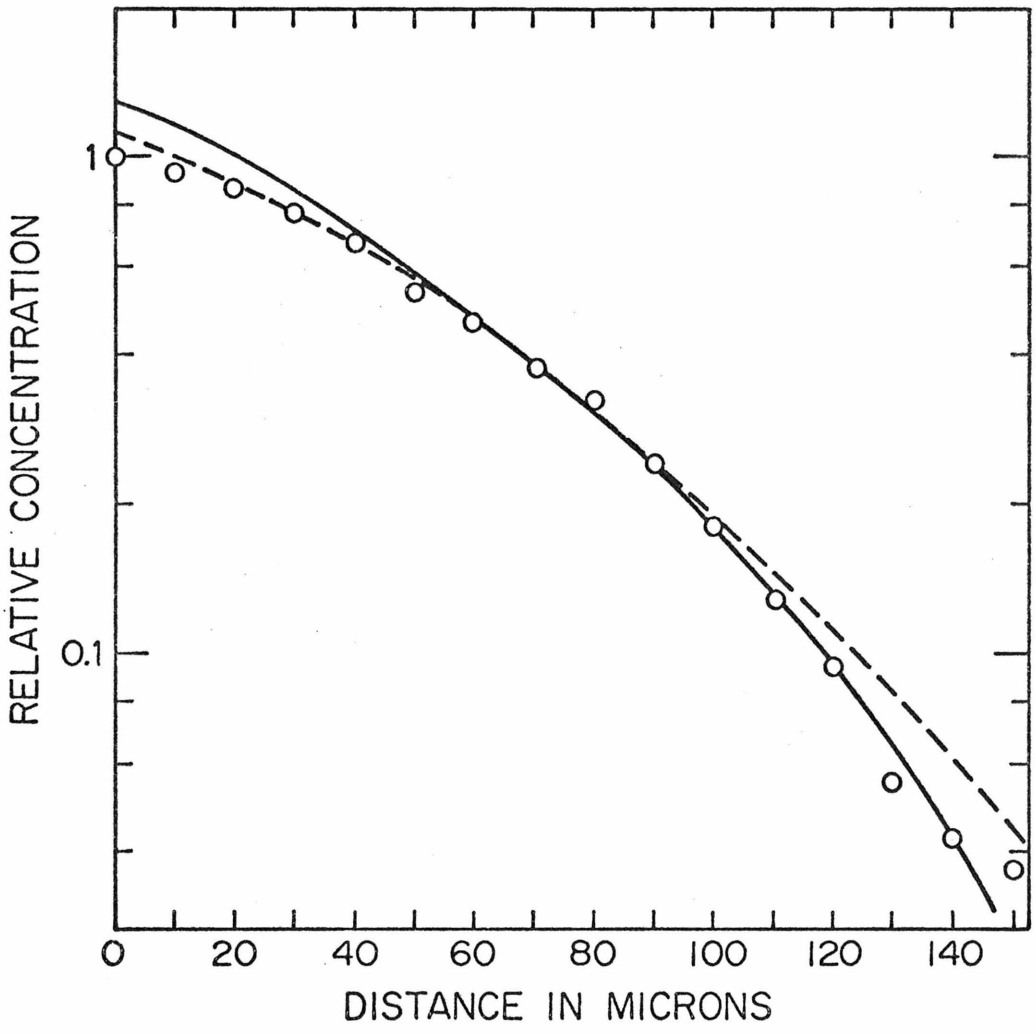
RELATIVE CONCENTRATION
1
0.1
0
20
40
60
80
100
120
140
DISTANCE IN MICRONS

The Si concentration values measured on the oxide cut or in the regions on the oxide immediately adjacent to the cut were taken as solubility values. The solubility values were corrected for absorption, fluorescence and atomic factor, as explained in more detail in Appendix 1.

B. Results and Discussion

1) Solubility - The solubility values of Si in thin evaporated Al films were found to be in essential agreement with the values reported in the literature (Fig. 4) for bulk Al [45-48]. Our values, however, show more scatter because of the uncertainty in locating the oxide cut boundary and because the Al on the oxide near the boundary had to be sampled. Si in solution in Al over bare Si tended to precipitate [8] and thus diffuse out of the reach of the electron beam. Thus solubility values measured on the oxide cut did not give reproducible results.

Our solubility data follow thermodynamic extrapolation more closely at low temperatures than the data of Dix and Heath [45] which are reported to be the most accurate by Hansen [7]. Thermodynamic extrapolation is done relying on a constant heat of solution. Their data show a positive deviation at low temperatures from a straight line fit to their data at temperatures above 400^{o}C. An estimate of the diffusion length obtained from the extrapolated diffusivity values and their reported annealing times indicates that the deviation cannot be accounted for by failure to reach equilibrium conditions. However, G. Tammann argued that actual solubility should be lower than the experimentally reported values on the basis that equilibrium is not reached at low temperatures in Al alloys [49]. In fact, solubility curves for several Al alloys show a break at a temperature near the

Fig. 4

Solubility of Si in solid Al according to previous investigators (curve) and our experiments (open circles).

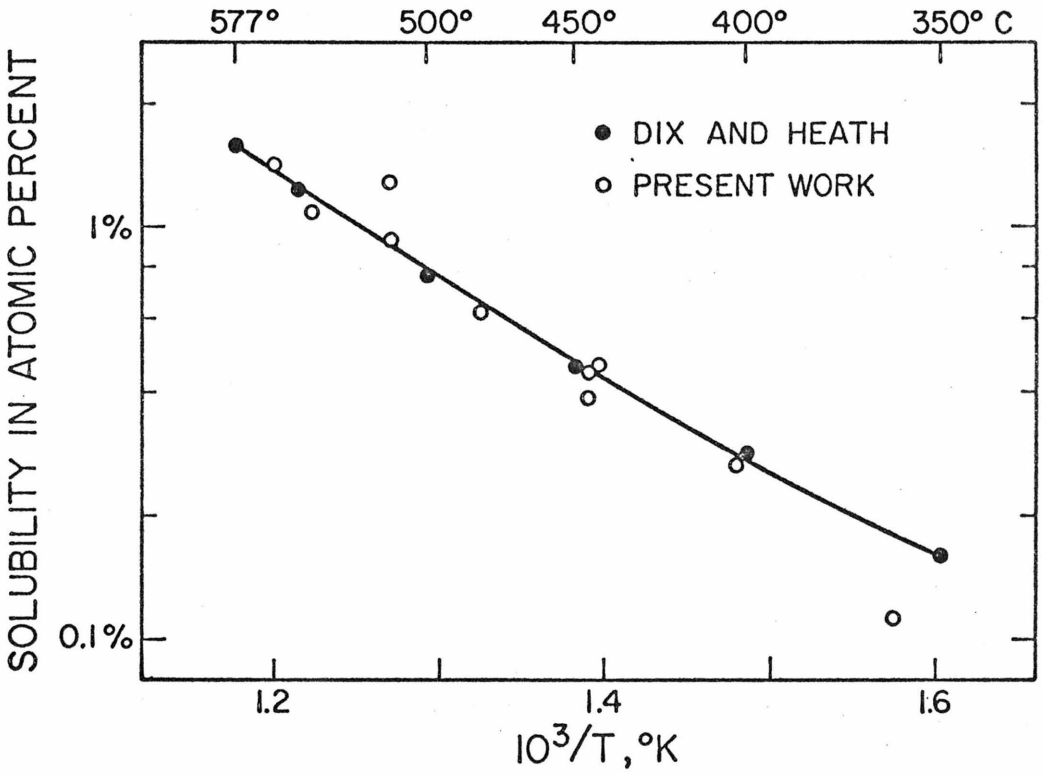
577°
500°
450°
400°
350° C
DIX AND HEATH
PRESENT WORK
SOLUBILITY IN ATOMIC PERCENT
1%
0.1%
1.2
1.4
1.6
10³/T, °K

recrystallization temperature of Al. This implies that cessation of mobility of Al atoms for grain growth and recovery accompanies the cessation of the mobility of solute atoms in bulk material. In view of the results of some investigators [47] who obtained solubility values at low temperature in defect-rich specimens, kinetics may have actually been the limiting factor in approaching equilibrium in bulk specimens.

Thermodynamic arguments can provide an alternate explanation for the above mentioned deviation. Thermodynamic calculations indicated that the Al-Si solution shows negative deviation from Raoult's law, and that the activity coefficient decreases with Si concentration [50]. Denoting the solubility by [Si] and heat of solution by ΔH ,

$$\ell n[Si] = -\Delta H/RT + C \tag{1}$$

where $\Delta H = \Delta G + T\Delta S$; but

$$\Delta G = \Delta G(\text{ideal solution}) + RT\{[Si]\ \ell n\ \gamma_{Si} + [Al]\ \ell n\ \gamma_{Al}\} \tag{2}$$

where γ is activity coefficient of the elements in solution. An activity coefficient close to but smaller than unity would produce the observed deviation.

Another approach bases on the hypothesis of the temperature dependence of the heat of solution. In fact,

$$\Delta H(T_2) = \Delta H(T_1) + \Delta C_p(T_2-T_1) \tag{3}$$

where ΔC_p is the difference of the heat capacity of the alloy and the heat capacity of the constituents obtained by algebraic addition of their heat capacities in their pure state.

$$[Si]_{Dix\text{-}Heath} / [Si]_{[const.\Delta H]} = \exp(\Delta C_p \Delta T/RT) \qquad (4)$$

whence $\Delta C_p \sim 3$ cal/g-mole/^oC at $T = 350^oC$, a rather large value that invalidates this explanation.

2) Diffusivity - Diffusivity values of Si in Al films are considerably larger than the values for wrought Al, as shown in Fig. 5. The diffusivity in bulk Al has been studied by chemical and spark spectrographic analysis [51], by electron microprobe analysis [52], by spectroanalysis alone [53-55], by microhardness measurements [56], and in sputtered films by precipitation rate measurements of Si using electrical resistivity data [43]. The data for bulk from various investigators show some scatter, possibly due to concentration dependence of D . In fact, Matano analysis performed by Mehl [51] and by Bückle [56] indicated that D decreases with solute concentration. Our diffusivity values for bulk Al agree with the values reported in the literature.

The diffusivity for thin films, however, are 1 to 1-1/2 orders of magnitude higher than bulk values. The more rapid diffusion of Si in Al films is due to the disordered structure of the evaporated matrix. This fact is also reflected in the lower activation energy or diffusion for thin films (0.79 eV) compared to 1.36 eV for bulk or wrought Al.

The evaporated film is polycrystalline and has structural defects. It consists of fine grains (e.g., [57]); it contains dislocations and dislocation loops [43], slip lines [58] and a large number

Fig. 5

The diffusivity of Si in solid wrought Al and evaporated Al. The filled symbols ● indicate the bulk values according to various investigators. The open symbols o indicate the values for evaporated films. For comparison, van Gurp's values for sputtered films are shown (dashed curve).

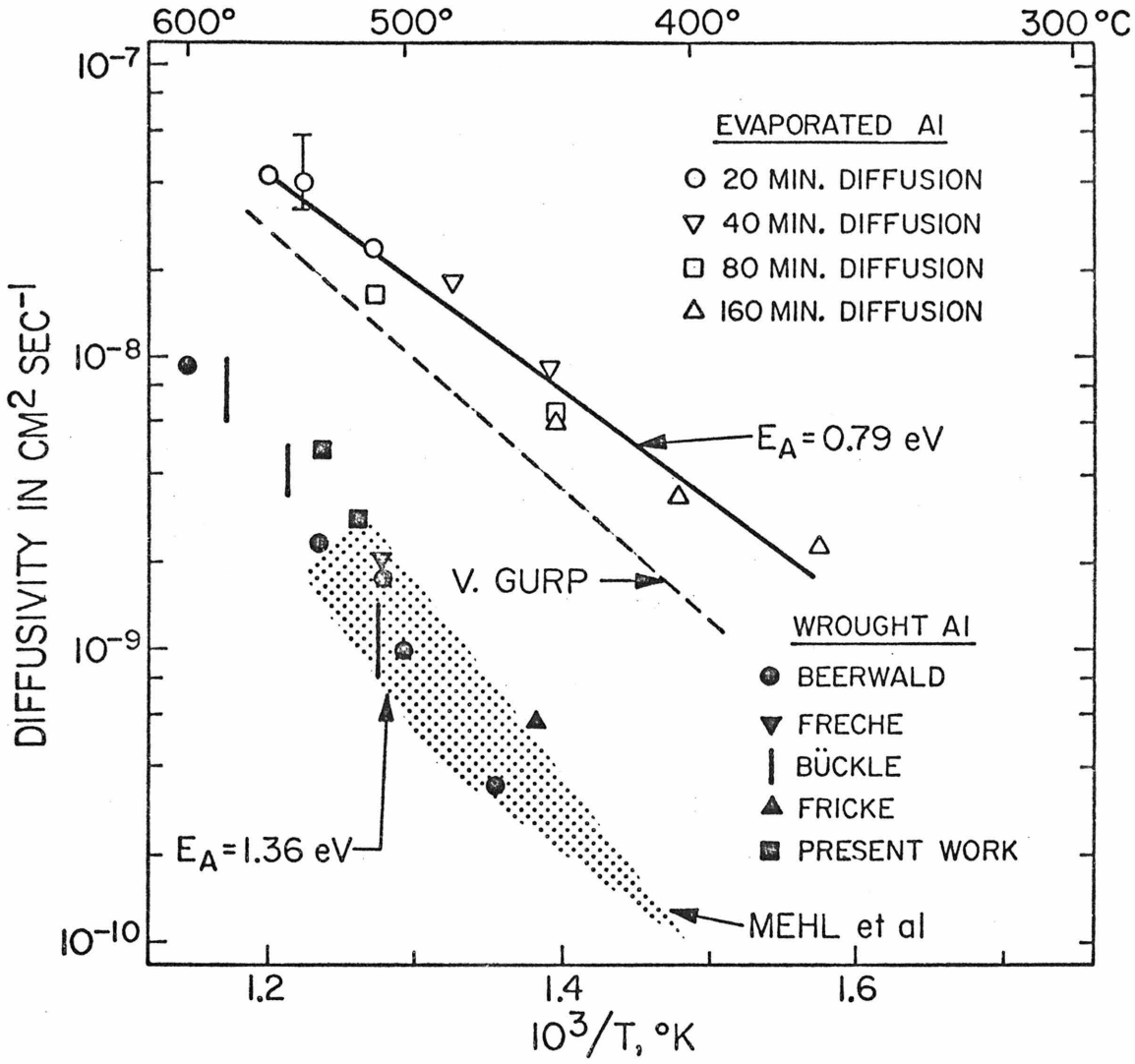
600°
500°
400°
300 °C
DIFFUSIVITY IN CM2 SEC-1
10-7
10-8
10-9
10-10
EVAPORATED Al
20 MIN. DIFFUSION
40 MIN. DIFFUSION
80 MIN. DIFFUSION
160 MIN. DIFFUSION
EA = 0.79 eV
V. GURP
WROUGHT Al
BEERWALD
FRECHE
BÜCKLE
FRICKE
PRESENT WORK
EA = 1.36 eV
MEHL et al
1.2
1.4
1.6
10³/T, °K

of quenched-in vacancies in the as-evaporated state. The quantitative distribution of these defects depends on the evaporation conditions such as substrate temperature, residual pressure of the vacuum system, deposition rate and subsequent annealing parameters.

The grain boundaries and dislocations are known to act as paths of rapid diffusion. However, diffusion along dislocations is the dominant mechanism in this system. TEM study of Al-0.8% Si sputtered films [43] indicated the presence of 10^{10} dislocations-cm^{-3}. These can be formed by plastic flow of the metal due to stresses arising out of differential thermal expansion of the film and substrate. About the same activation energy for Al self diffusion along dislocations was found by Volin et al. (0.85 eV) [59].

The grain boundary diffusion cannot be ruled out on the basis of the above presented data, since the activation energy should be about the same. However, the grain size ($\bar{r}$) necessary to provide equal cross sectional area of fast diffusion path can be estimated, assuming columnar grains with boundaries normal to the surface and one atomic diameter (a_o) boundary width [60].

$$10^{10}[\text{disl-cm}^{-3}] \times a_o^2 = 10^{-4}[\text{cm, film thick}] \times a_o \times \bar{r} \times \left(\frac{1}{r^2}\right)[\#\text{ of grains}]$$

$\bar{r} \sim 30\text{Å}$ an excessively small value. Microscopic analysis of our specimens revealed that the grain size was 3-10μ. Grain growth is expected to occur in specimens annealed at temperatures above 200°C [61]. The effect of long annealing in our specimens has been measurable but small enough to rule out this explanation. On the other hand, should the

grain boundary diffusion be predominant, the discrepancy between bulk and thin film diffusivities is expected to disappear at temperatures close to the eutectic point, but such is not observed.

The hypothesis of Si vacancy pair diffusion can be similarly discarded, since annealing would have eliminated the excess vacancy concentration by sinking them in dislocations.

Structural defects such as slip and dislocation lines are likely to be produced in large quantities because of working of the Al film by thermal stresses [62]. An estimate of the thermal elastic stress in the Al film near the Al-Si interface would give

$$S = Y_{Al}(a_{Al} - a_{Si})\Delta T/(1-\nu) \sim 10^9 \text{dyn/cm}^2 \qquad (5)$$

where a is the thermal expansion coefficient, Y and ν are Young's modulus and Poisson's ratio for Al at this temperature. This value exceeds the elastic limit of Al and will cause plastic flow by shear [63]. Our activation energy for diffusion is in essential agreement with the values reported by v. Gurp [43] (.85 eV for 0.4% Si and .90 eV for 1.8% Si) for sputtered films. The activation energy estimated from Si precipitation studies in 11% Si-Al splat-cooled samples [64] are within 10% of the above mentioned values (0.61-0.87 eV). These represent heat of diffusion if diffusion limited precipitation is also a valid model for splat-cooled films. A close agreement is also found when the calculated activation energy for Si-vacancy pair migration (0.82 eV) [65] is compared to experimental values. However, the energy of diffusion involves Si-vacancy pair binding too, which lowers the

last cited value to .54 eV when solute-vacancy pair migration is assumed to be the predominant mechanism.

There was scatter in our diffusivity data, the worst case of which is shown in Fig. 5 for D at 540°C. The error may have been due to uncertainty in the determination of the origin for reasons mentioned in the "solubility" section. Another reason is the fact that the Al film on the cut, the source for Si, was not saturated with the solute in the regions bordering the cut boundary, which is a slight perturbation on the assumed mathematical model.

3) Conclusion - The solubility and diffusivity of Si in thin vapor deposited Al films have been investigated by electron microprobe analysis. The solubility values are in essential agreement with bulk value, whereas diffusivities are found to be considerably larger than in wrought Al. The 1 to 1-1/2 orders of magnitude enhancement is due to the presence of large numbers of dislocations present that form "diffusion pipes" for Si. In this investigation the local microanalysis capability of the electron microprobe was exploited and applied for the chemical analysis of thin films.

The enhanced diffusivity values are in between those observed for metallic impurities in Si and diffusivities in the liquid state (Fig. 6). In the fabrication of doped layers the growth rate of Si epitaxial layers in thin metal films is then more rapid than conventional diffusion of impurities into Si for the same temperature range. The advantage of higher diffusivity in liquid state, on the other hand, is offset by smaller diffusion lengths in solid state. These

Fig. 6

The diffusivity of Si in solid Al, compared to the diffusivity of common dopants in solid Si and diffusivity of Si in liquid metals.

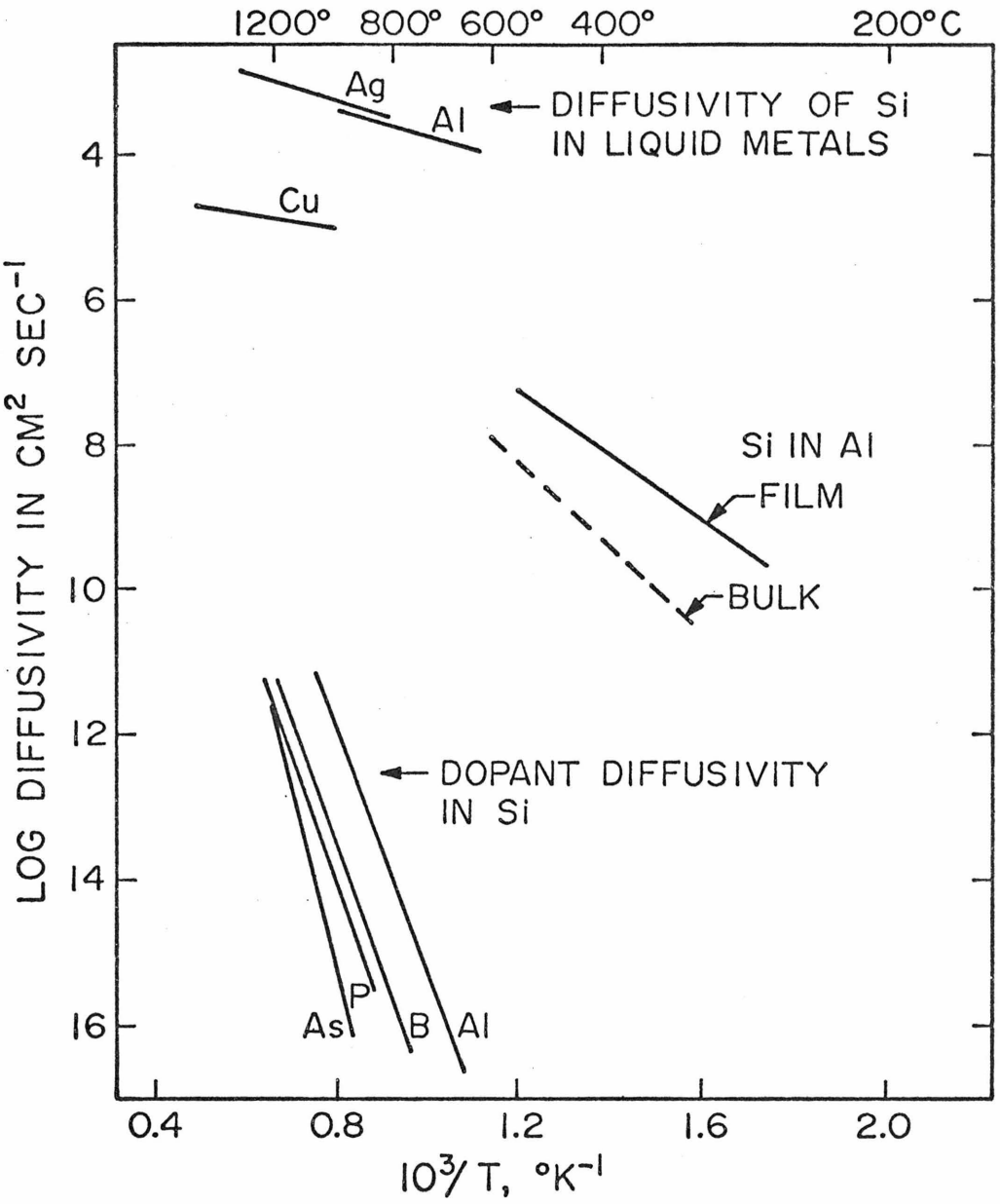
1200° 800° 600° 400° 200°C
Ag
Al
DIFFUSIVITY OF Si IN LIQUID METALS
Cu
Si IN Al
FILM
BULK
DOPANT DIFFUSIVITY IN Si
As
P
B
Al
LOG DIFFUSIVITY IN CM² SEC⁻¹
4
6
8
10
12
14
16
0.4
0.8
1.2
1.6
2.0
10³/T, °K⁻¹

considerations make thin metal films a suitable medium for epitaxial growth as far as transport of semiconductor solutes are concerned.

III. PRECIPITATION OF Si IN THIN Al FILMS

As discussed in the "solubility" experiments, Si in solution in Al tended to precipitate upon cooling unless special precautions were taken. Analogous conditions prevail during device manufacture which should allow precipitation and growth of Si crystallites. Therefore, an investigation of Si precipitation behavior in Al films was undertaken.

A. Sample Preparation and Analysis

Preparation of the specimens was identical except for annealing to those for diffusion studies as explained in the previous section. The specimens were annealed at 530°C for ∿ 1 hr with the intention of saturating the Al metallization with Si. Thereafter they were either quenched or cooled at a rate of 10°C/min until 275°C. A class of specimens was aged for 15 or 60 sec at 435°C by placing them in a cavity in a preheated Cu block immediately after the long anneal at 530°C. The slow cooled or aged specimens were quenched from their respective final temperatures by dropping them onto a cool asbestos surface.

The analysis was performed with an electron microprobe, with a finely focused (0.2μ diameter) beam. The beam energy (10 keV) was such that it excited Si only in the Al film (Fig. 7a). Either counts were taken at specific locations and intervals, or the specimen was displaced laterally with respect to the electron beam in a direction perpendicular to the cut boundary at fixed speed to obtain a continuous Si distribution profile (Fig. 8). A different mode of operation

Fig. 7

a) Cross sectional view of the specimens, schematized to illustrate the experiment. b) Top view of the specimen as exhibited on the CRT screen by the electron microprobe tuned to SiKα fluorescence. Si precipitates in the Al films appear as white particles. This specimen was allowed to cool down at 10^{o}C/min rate from the annealing temperature. c) Micrograph obtained by the same technique as a specimen that was quenched. The horizontal distortion of precipitate shape is an artifact arising from the resolution time of the scanning electronics.

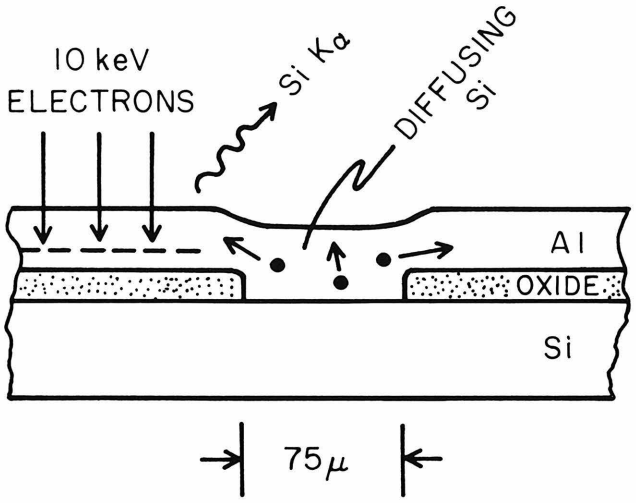

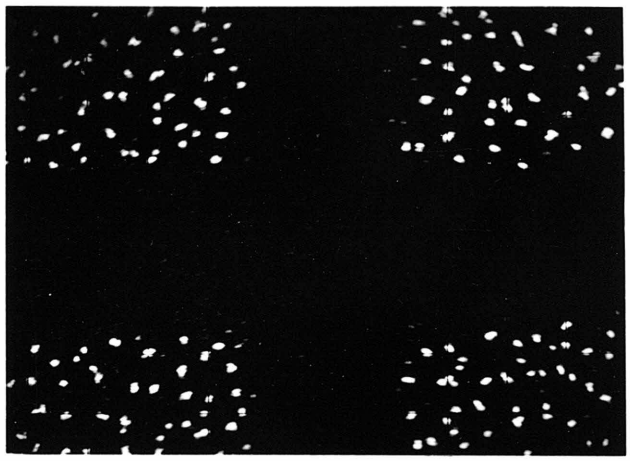

AFTER SLOW COOL

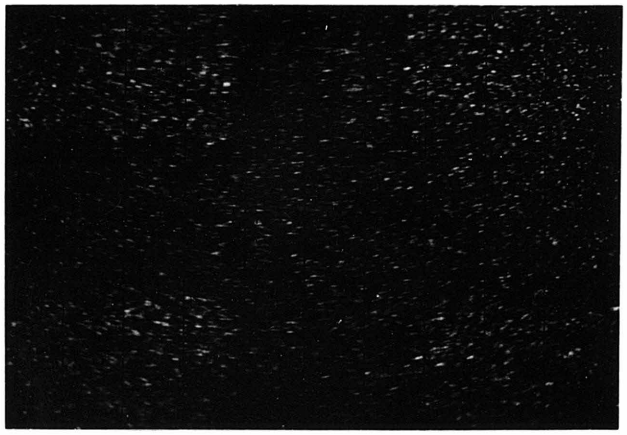

AFTER QUENCH

was exploited when the beam scanned the surface in a raster and the $Si_{K\alpha}$ signal was used to modulate the electron beam intensity of a CRT. The information on spatial distribution of Si was thus displayed on CRT screen, where the spot intensity was in semiquantitative correspondence to Si concentration.

B. Results and Discussion

Figures 7b,c and 8 show Si distribution in Al film under quench and slow cool treatment. The precipitation took place on the Si-Al interface when this was readily accessible as it is on the cuts. In this case, the Si atoms are outside the excitation volume of the beam. In places where Si surface was covered with oxide, Si precipitates grew in the Al film near its free surface. The depth distribution of precipitates was obtained by probing the film with increasing beam voltages, hence increasing penetration depths.

Some Si is retained in solution (Fig. 7b) even on the cuts under aging and quench or simply quench conditions, which in our case corresponded to cooling at a rate of 10^2 °C/sec. This result can be explained by comparing the diffusion length (L) of Si in Al with the film thickness

$$L = \left\{ \int_0^{t_o} D[T(t)]\, dT(t) \right\}^{1/2}$$

where t_o is the cooling period. Using the approximation $L \sim \sqrt{<D>t}$, where $<D>$ is the average diffusivity over the temperature interval, one estimates 1μ for L for quench conditions. Thus only a fraction of Si is able to diffuse to the Si-Al interface. Under slow cool

Fig. 8

Profile of Si concentration in Al across a cut in the oxide (shown by the 50μ marker). Microprobe traversing speed was 55μ/min.

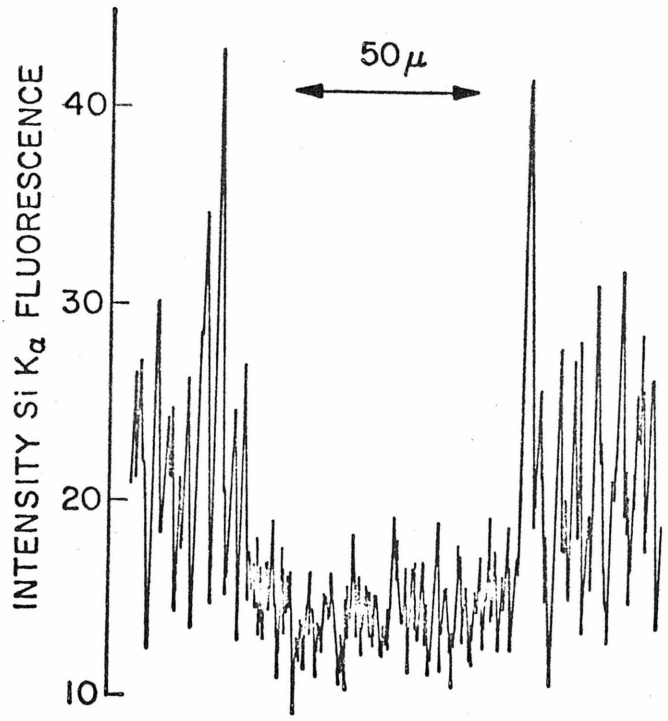
50μ
INTENSITY Si Kα FLUORESCENCE
40
30
20
10

conditions there is ample time for Si to reach this interface.

Previous investigations on Al-Si alloys had indicated the importance and role of excess quenched-in vacancies, in the nucleation of Si precipitates [65,66]. The vacancies were found to cluster in dislocations which form nucleation sites for Si. However, the precipitate crystallites that survive the nucleation phase and coarsen are those which minimize the strain and interfacial energies. Thus an important fraction of precipitates in the film over SiO_2 grow along grain boundaries and triple points in cylindrical forms with their axes normal to the substrate [43]. The tendency to grow near the free surface of the film is to be expected, since this portion of the film can flow unconstrained and accommodate stresses arising out of crystallization of Si precipitates.

The growth of Si over the Si-Al interface occurs because the substrate is a good nucleation site. The energetics for this type of growth is favorable, especially at small precipitate sizes, since interfacial energy is only that due to any additional interface formed because of the non-smooth nature of growth structures. However, growth of columnar Ge or Si crystallites in highly supersaturated Ge-Al, Si-Ag films [15] indicates that interfacial energy contribution may be small.

C. Conclusion

Microprobe analysis of Si precipitation in Al films indicated that the Si substrate surface acts as an effective nucleation center. The Si in solution, one diffusion length away from the Si surface, forms precipitate lumps near the free surface of Al that coarsen with time.

IV. SOLID PHASE EPITAXIAL GROWTH OF Si MESAS IN Al METALLIZATIONS

A. Sample Preparation and Analysis

Samples were prepared with 1-10Ω-cm p or n type Si wafers with their surfaces normal to (111) direction. One side of the wafers had been polished by Monsanto Co. with Syton. A thermal oxide 0.3μ thick was grown and cuts of various shapes and sizes were etched in it photolithographically.

The specimens were loaded in the vacuum system after being dipped in dilute HF, rinsed and dried. A layered structure consisting of 10μ Al, 200-1000Å Si, and 10μ Al was vapor deposited at a pressure of 10^{-6}-10^{-7}torr from a three crucible electron gun evaporator. The extra thickness of the films allowed us to grow large enough structures that could be studied in detail. The heat treatment of the specimens was done in dry N_2 atmosphere. Some of the specimens were annealed at 540°C for 5 min and then allowed to cool down in the furnace at the average rate of 3°C until 150°C. Others were subjected to a 13 hr isothermal treatment at 540°C and quenched at the termination of annealing. The Al film was then removed in phosphoric acid at 65°C which left Si and SiO_2 intact. The specimens were then subjected to SEM analysis without application of a conductive coating.

The scanning electron microscope is an analysis tool, sensitive to surface structure. The operation is based on irradiating the sample surface with an electron beam in the keV range, and collecting the secondary or the backscattered electrons, which then modulate the beam

intensity of a CRT. Thus visual inspection of the surface can be accomplished at high magnification, with high resolution and depth of field.

B. Results and Discussion

The optical and scanning electron microscope study of the specimens revealed a variety of growth structures, depending on the supersaturation level of Al with Si and annealing conditions. The presence of the evaporated Si which is known to be amorphous [67] in the Al film prevented any noticeable dissolution taking place from the wafer substrate. The evaporated layer dissolved and saturated the Al film on account of the higher free energy of the amorphous state. This allowed us to observe growth structures distinctly, since these occurred on a flat smooth surface.

At low supersaturation levels and slow cooling the most common structures were mesas, on the average 5μ wide, 2000Å high, interspersed on the Si surface as shown in Figs. 9 and 10. The oxide-Si step seems to be a preferred site for this type of growth, as will be explained later.

Figure 11 shows that mesas have a definite orientation within each Al grain, with their long dimensions all pointing approximately parallel in a given direction.

Fewer in number but larger and often faceted mesa structures were observed when the specimens were subjected to long isothermal annealing (Figs. 12,13). Some low profile faceted structures measured 80μ in their long dimensions. A combination of the two structures was

Fig. 9

SEM micrograph of Si mesas grown onto the exposed substrate Si (cross region). Tilt angle, 65^{o}. The oxide is still present at the corners. Note that the oxide-Si step is a preferred growth site for mesas.

Fig. 10

Close-up view of mesas in a region different than in Fig. 9.

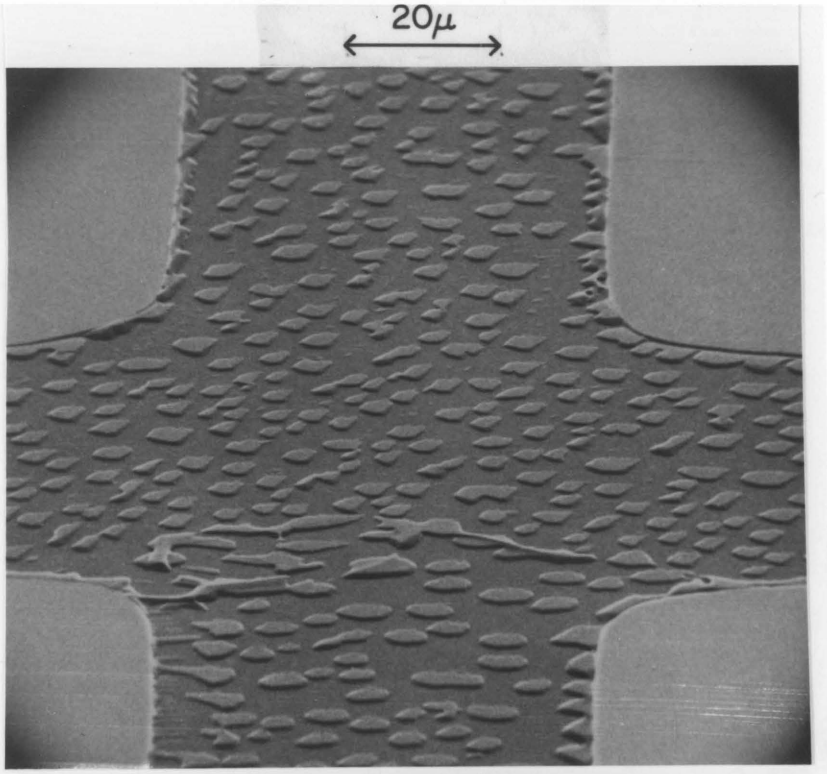
20μ

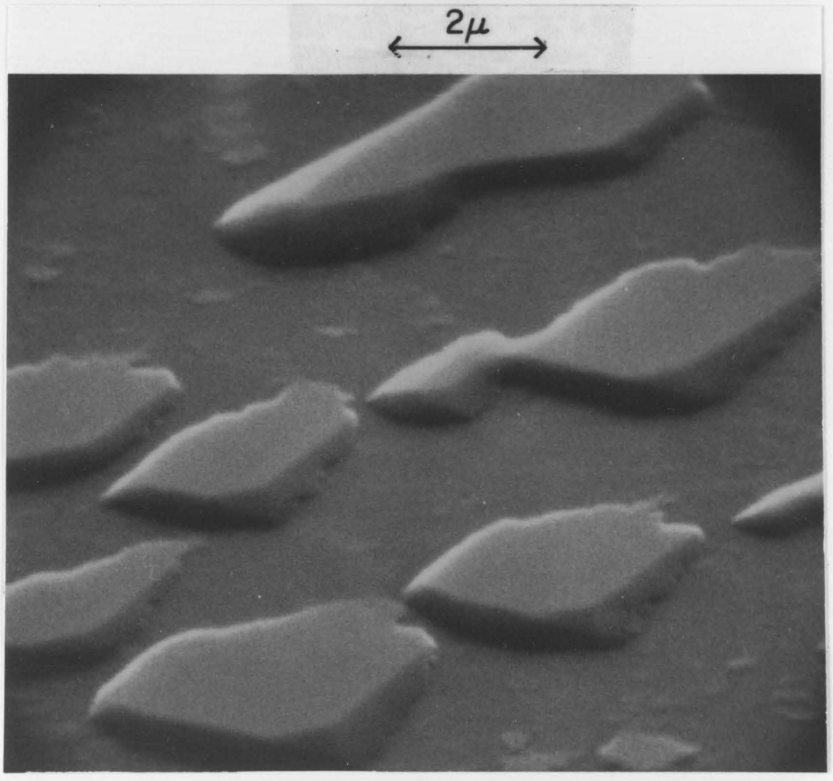
2μ

Fig. 11

Faceted, low profile structures as exhibited by SEM. The growth took place on (111) Si substrate, under isothermal treatment of a slightly supersaturated specimen.

Fig. 12

Faceted structure grown under similar conditions on (100) Si substrate. Note that faceting reflects crystalline symmetry.

10 μ

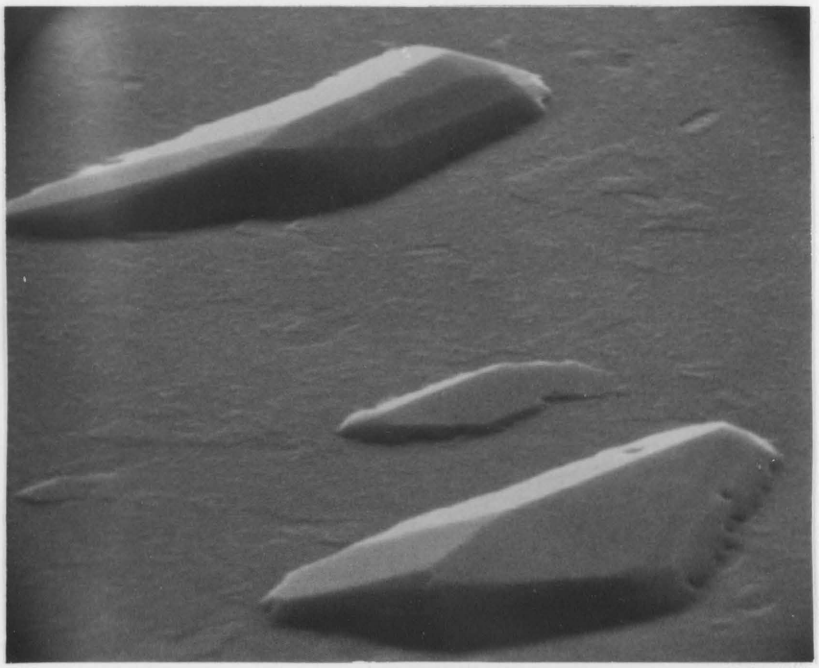

2 μ

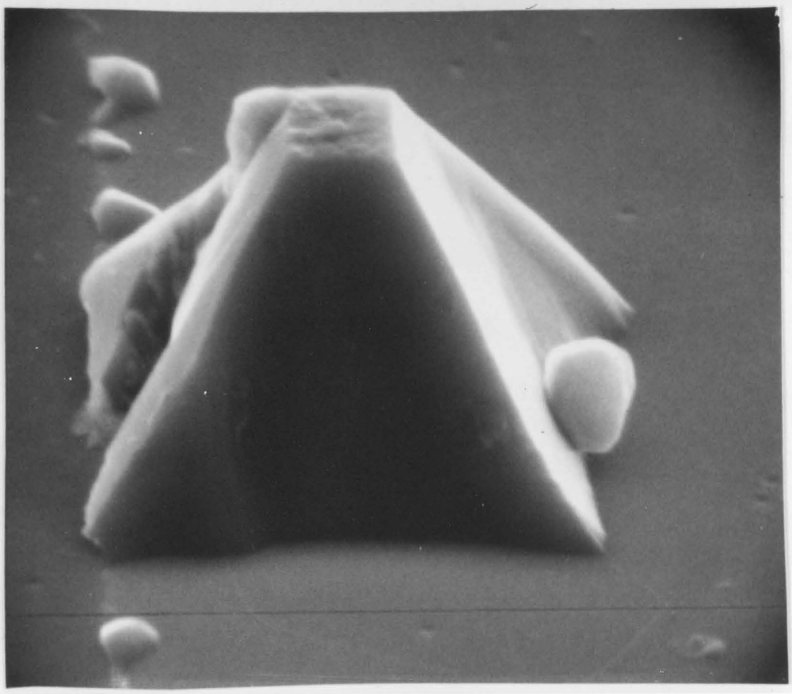

observed when treatment of the specimens consisted of long isothermal treatment followed by slow cooling. Some islands were in the form of low angle ramps, with a common orientation. This may reflect effects of deviation of the substrate from (111) orientation [68] and interfacial energy of Si-Al crystals.

At high supersaturations (2-5% Si) the structures consisted of 10-30μ wide flat plateaus separated by canyons which correspond to the position of grain boundaries in the Al film (Fig. 14). Often vertical membrane-like growths developed in the middle of the canyons, which is a growth feature also observed by other investigators [43].

A noteworthy aspect of mesa growth was observed under slow-cool conditions when the growth region was limited to an oxide cut a few microns in diameter (Figs. 15-18). Figures 17 and 18 show that growth proceeds from the reentrant corners--the oxide step--towards the center. The tendency of growth to occur at such reentrant corners can be explained by consideration of stresses in the Al film. These regions are expected to produce a larger amount of tension locally in the Al film during cooling because, as the film contracts, it adheres both to the substrate and the oxide walls. The tension can be partly relieved if Si in solution precipitates and thus occupies a larger volume in crystalline form than in solution. Figure 18 shows the growth structure when the substrate--even in the cut--was thermal oxide. Again, a step allows growth even in the absence of epitaxy over the surrounding flat regions.

Fig. 13

Growth structures on Si in a region where three grain boundaries in Al intersect. The mesas exhibit a definite orientation within each grain.

Fig. 14

SEM picture of large growth plateaus and membrane-like structures between these, in a supersaturated specimen. Al is stripped off by etching in all samples analyzed by this method.

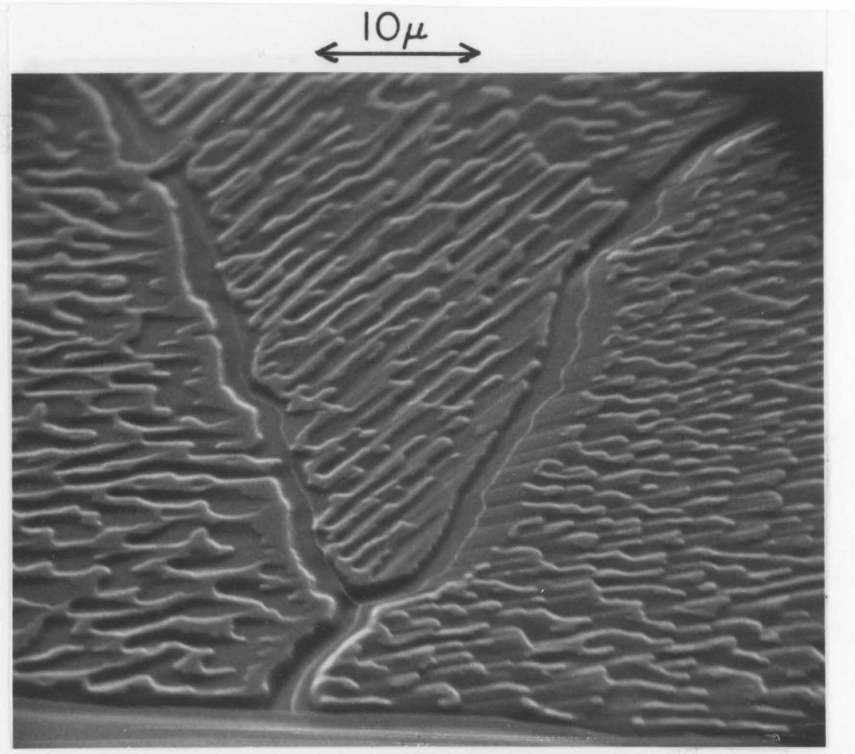
10μ

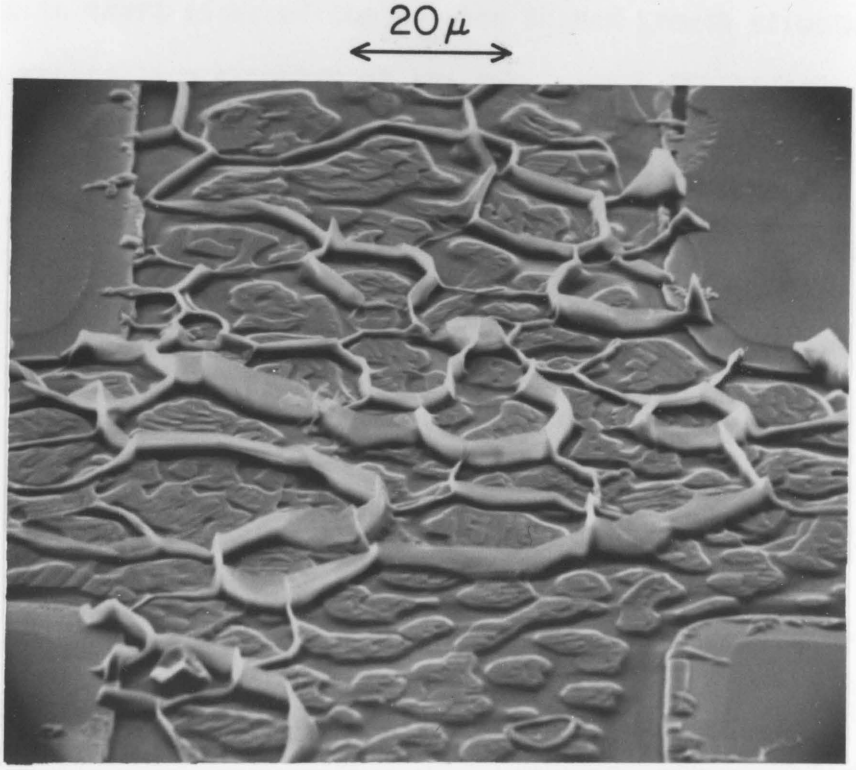
20μ

Fig. 15

SEM picture of a mesa grown in a 4 x 4μ oxide cut

Fig. 16

Same as Fig. 15, except the oxide cut was 4 x 8μ . Faceting, evident in short sides of the polygon shaped growth structure, reflects crystalline symmetry of the substrate. The sides are parallel to 111 planes.

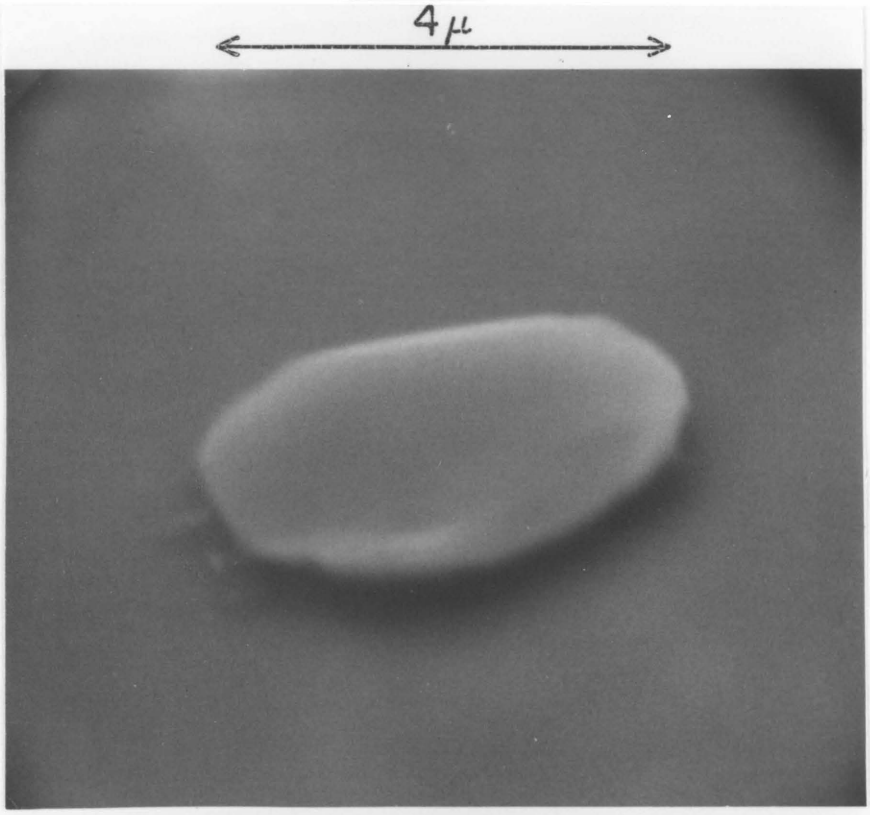
4μ

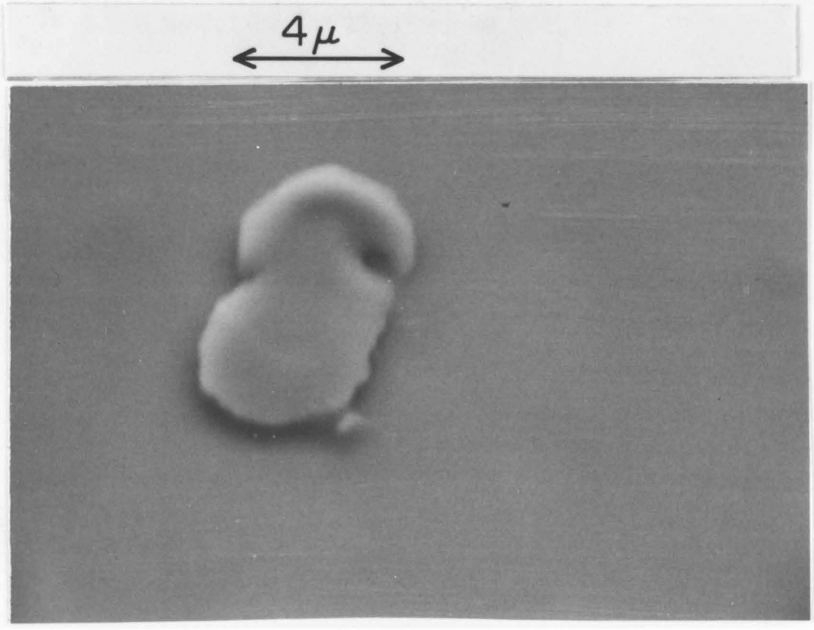
4μ

Fig. 17

Same as in Fig. 15. The faceting as well as the tendency of growth to occur at oxide steps can be seen.

Fig. 18

Si growth structures in a 5μ x 5μ depression in SiO_2. The bottom of the cut is also covered by thermal oxide.

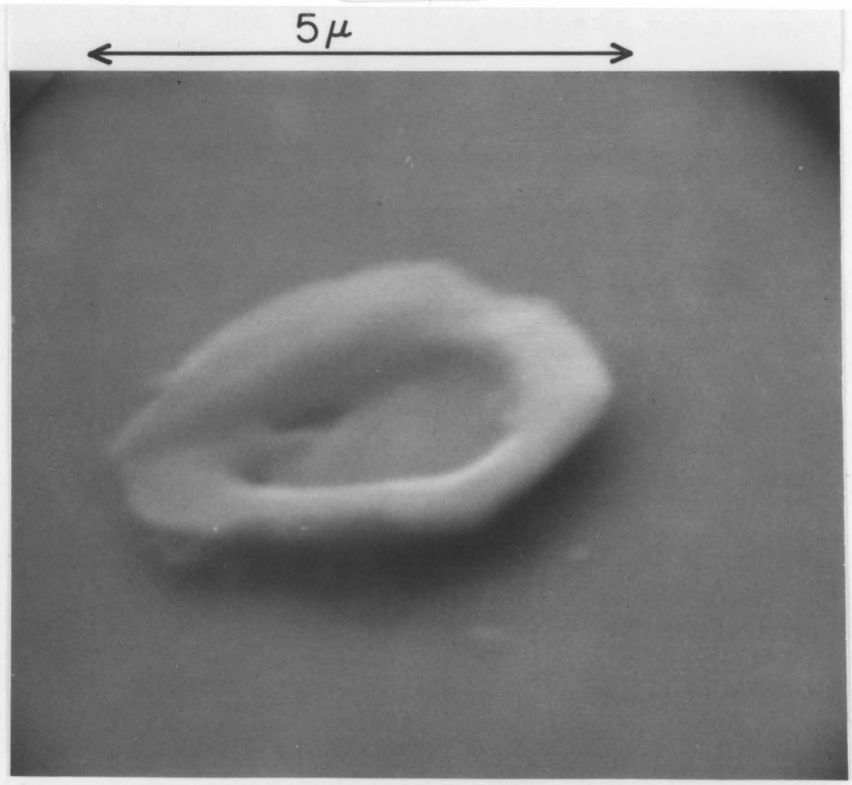
5μ

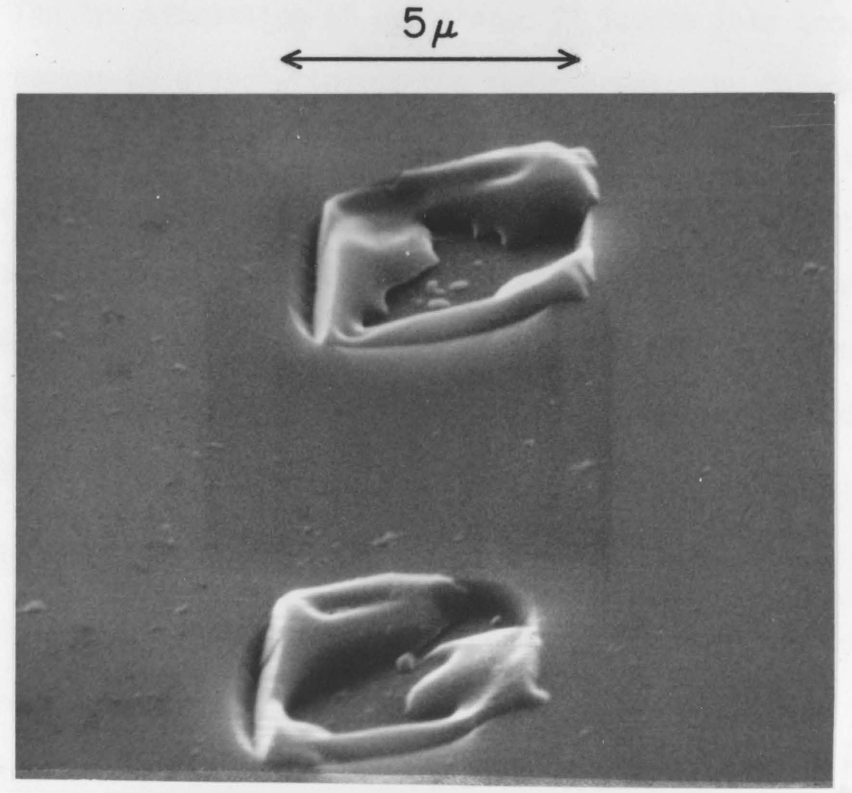
5μ

Figures 15-17 show hexagonal faceting in these growth structures. The facets align with (111) orientation of the substrate crystal in agreement with the epitaxial orientation found in channeling studies for the Ge-Al system [36]. The epitaxy of these structures was confirmed by He^+ backscattering channeling measurements in some specimens.

Among the above-mentioned growth structures, the mesas that completely fill holes in the oxide are potentially useful for device applications. One can envision growth of localized p-type Si mesas for such applications as diode array targets, cold cathode structures, negative electron affinity devices. In fact, liquid phase epitaxy [69] or vapor phase epitaxy [70] have been used to produce similar raised p-type structures for such purposes. The elevation is necessary to prevent charging of the surrounding oxide by the electron beam.

The transformation of evaporated Si layers into growth structures proceeds by dissolution of the semiconductor by the metal, transport to the nucleation site and growth of epitaxial crystallites. The driving force for this mechanism is the higher free energy of the amorphous Si compared to crystalline Si. However, it is shown that mechanical strain also plays a role. Other forces, like temperature gradient, are also likely to induce transport and growth under suitable conditions.

C. Suggestions for Further Study

The morphology of the growth is likely to be affected by surface cleanliness and defects. Recent work [84] on the extensive dissolution of Si into Al may elucidate the effectiveness of this interface reaction

in producing a surface clean of native oxide, residues of polishing and chemical treatment. In fact, in the growth of epitaxial layers by liquid or vapor phase epi, limited dissolution of the substrate is allowed to obtain a clean surface in atomic scale. Similar practice is known to produce better adhesion of certain metals deposited by vapor phase transport and reaction of their halides on Si [71] and superior crystalline quality for Si epitaxial growth on insulating substrates, when the latter are etched at high temperatures with H_2.

The preparation of the Si surface by chemical etching (using Si halides at elevated temperatures), by sputtering [72] before metal deposition or by extensive dissolution reaction with Al films, may produce larger and more uniform structures that are more suitable for device fabrication. Mayer et al. [39] have shown that chemical reaction of Pd with Si to form Pd_2Si accomplishes the above surface preparation for epitaxial growth.

Information on structural perfection of the growth structures as well as nucleation sites of the mesas can be obtained by transmission electron microscope studies. Structural defects of the substrate, such as terminals of screw dislocations, steps, kinks, are likely sites to nucleate the observed growth structures.

The doping level of these structures can be analyzed by secondary ion mass spectroscopy (SIMS) or proton resonance profiling (PRP) methods.

SIMS bases on continued removal of the substrate by sputtering and performing mass analysis of the ionized sputtered particles. The sensitivity for Al in Si is on the order of 0.1 ppm. The mass analysis

is such that good sensitivity can be obtained for the individual isotopes of Si and Al. Although this method will be useful to obtain the total Al concentration, nonuniformity of the sputtering rate may make it inadequate for concentration profiling.

If the concentration is as high as reported [73], then PRP can be used to obtain concentration profiles of dopants with depth for various growth conditions. PRP bases on detection of proton capture resonance reaction, which in this case will be [74,75]

$$^{27}Al(p,\gamma)^{28}(Si) \qquad (6)$$

D. Advantages of Solid State Epitaxial Growth

The advantages of solid phase epi growth over vapor or liquid phase growth [76-78] or growth from a gel [80] are the ability to maintain dimensional control of structures and lowering of the growth temperature.

Dimensional control is possible because solid phase growth is a diffusion controlled slow growth process. This is brought about by the fact that very dilute solutions are used and transport occurs by solid state diffusion.

In the case of Al-Si, the growth is estimated to proceed at the rate of 0.1 - 1μ/hr at 400°C and 500°C respectively, in our experimental conditions. This rate is low when compared to a typical figure of 10-100μ/hr in the liquid and vapor phase epitaxy, and 1-2 cm/hr in the growth from a stoichiometric melt, where the growth rate is mainly determined by the removal rate of the heat of solidification from the

freezing interface. Fine dimensional control is also facilitated because of the absence of the surface tension of the liquid phase.

The diffusion limited nature of growth, which renders near equilibrium conditions in the vicinity of advancing growth interface, should eliminate dopant concentration variations. Needless to mention, such phenomena as constitutional supercooling do not exist in solid phase growth.

The thickness can, in principle, be controlled by the amount of vapor deposited Si, provided the ratio that is transported and regrown versus that which remains in the metal film is known.

The lower growth temperatures should provide higher crystalline perfection. At high temperatures, which are used for conventional vapor phase epitaxy or diffusion, plastic deformation occurs. In addition, large stresses build up during cooling which cause formation of slip and dislocation lines, especially at junctions of differently doped regions. These are known to getter metallic impurities and cause serious leakage problems. The stresses are greatly reduced when the growth temperature falls to $500^{o}C$ or less.

There should be a substantial reduction in the number of quenched-in vacancies for the low temperature growth. In fact, assuming 2.32 eV for the heat of formation of Si vacancies [83], the ratios of the number of vacancies in the Si crystal grown at 500^{o} versus that grown at $1100^{o}C$ (for vapor phase) and at 1430^{o} (growth from melt) are 3×10^{-7} and 5×10^{-9} respectively. Dislocation density should similarly be lowered by several orders of magnitude.

E. Conclusion

Growth of Si epitaxial structures in solid phase in Al films was studied with the SEM. A variety of growth structures, including mesas, faceted structures, large flat plateaus, were observed depending on the Si content of the Al film and annealing conditions. More work needs to be done to produce large-scale uniform structures.

V. THE EFFECT OF PRESSURE ON THE SOLID PHASE EPITAXIAL GROWTH OF Si

The effect of mechanical pressure as driving force on the dissolution and growth of Si epitaxial structures was investigated by means of the SEM. The application of nonhydrostatic pressure is a feature peculiar to solid phase growth, since fluids cannot support appreciable pressure differences.

A. Sample Preparation and Analysis

The samples were prepared using n or p-type Si dice, the surfaces of which were normal to (111) direction. Al or 99.999% purity was evaporated from a W crucible in an electron gun equipped vacuum system. The film thickness was 10μ. The actual samples, about $4mm^2$ in area, were cleaved from these dice.

A counterplate in the form of a waffle iron was prepared to apply differential pressure (Fig. 19a). This plate was fabricated by etching deep grooves into a Si wafer using Au film as the masking metal layer, and using conventional photolithography to define the pattern on the Au film. The plate was then subjected to thermal oxidation. The samples were annealed at $540^{o}C$ for 13 hr, with an applied pressure of 40-100 atu. At the removal of the pressure, the annealing was also terminated by quenching. The Al film was removed in hot phosphoric acid and the sample subjected to SEM analysis.

The specimens with n-type Si substrate were investigated with voltage contrast mode of SEM. Electrical contacts to these samples were

made by evaporating 4 mil Al contact pads and bonding Au leadwires to them. The samples were then mounted in a decapped TO-5 header.

Voltage contrast mode of SEM bases on the fact that application of a small bias to the specimen affects the secondary electron collection efficiency, since the collector is only a few volts positive with respect to the specimen.

B. Results and Discussion

Microscopic observation of specimens revealed that the topology of the pressure plate was replicated on the specimen. SEM analysis indicated that raised structures had formed on the specimen corresponding to grooves on the pressure plate. Square shaped depressions were seen between these, corresponding to parts of the plate that were in contact with the film. Figures 20 and 21 show top and cross sectional views of the raised structures that measure 2000-5000Å. As can be seen from the figures, the surface is not smooth; however, there was no ambiguity in the relative elevation of structures.

Figures 19b,c show voltage contrast SEM study of these structures. The difference in contrast at the application of reverse bias is an indication of an n-p junction between the substrate and the raised growth structures. The negative potential of the latter structures results in larger secondary electron collection in SEM, which gives them greater brightness. This is a proof that these structures are p-type Si.

The position of the p-type growth structures with respect to the cuts in the pressure plate indicates that growth must have been dominant

Fig. 19

a) Schematic of the "waffle-iron" compression plate and plain specimen. b) Appearance of the specimen in the SEM after pressure-temperature treatment, with no applied voltage. c) Same as in b, except -1.8V bias is applied on Au bond. A mesa was etched in the specimen to electrically isolate a relatively small area. Dark regions are grounded and bright regions have negative bias.

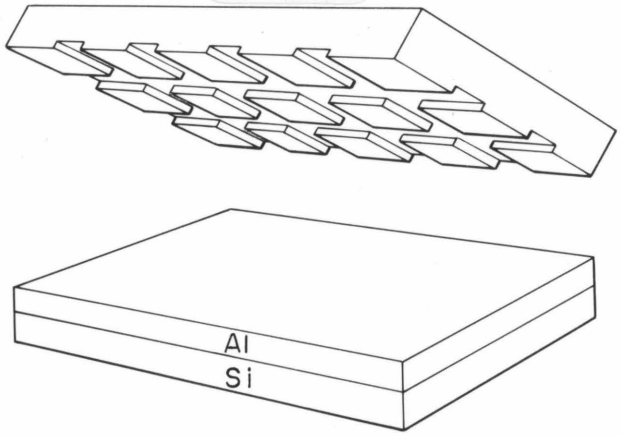

SCHEMATIC

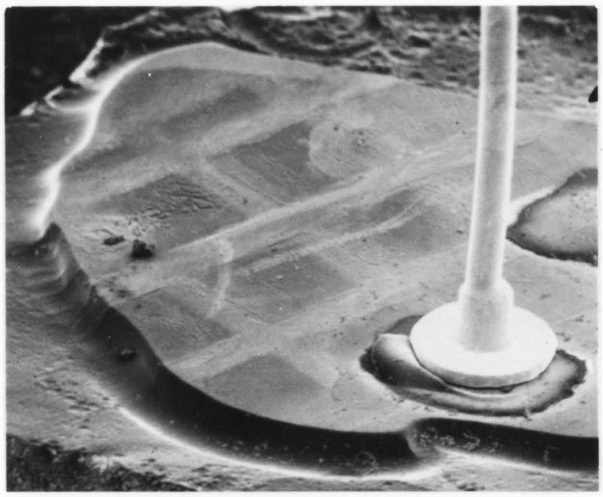

NO APPLIED VOLTAGE

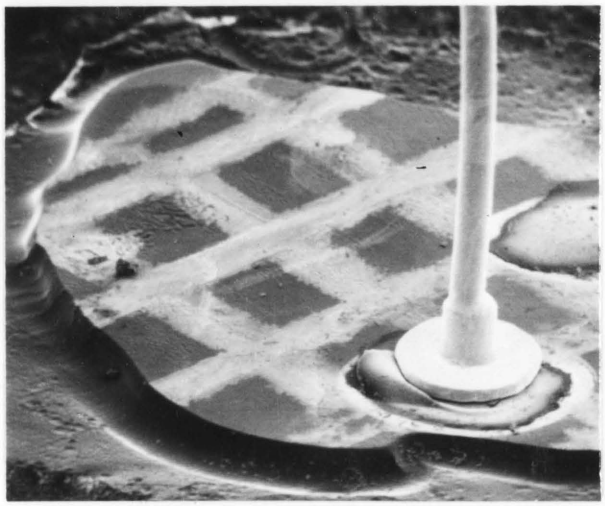

-1.8V ON Au BOND

Fig. 20

Growth structure (cross shaped) on the specimen after pressure-temperature treatment, as exhibited by SEM after removal of Al film.

Fig. 21

Cross sectional view of the growth structure, as in Fig. 20, observed at the edge of the specimen.

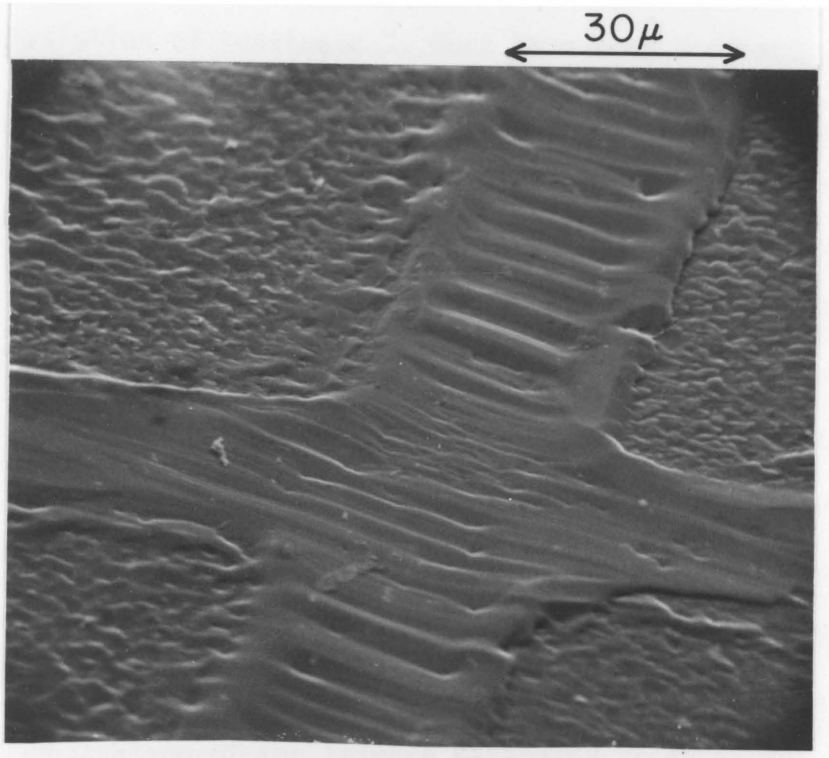
30μ

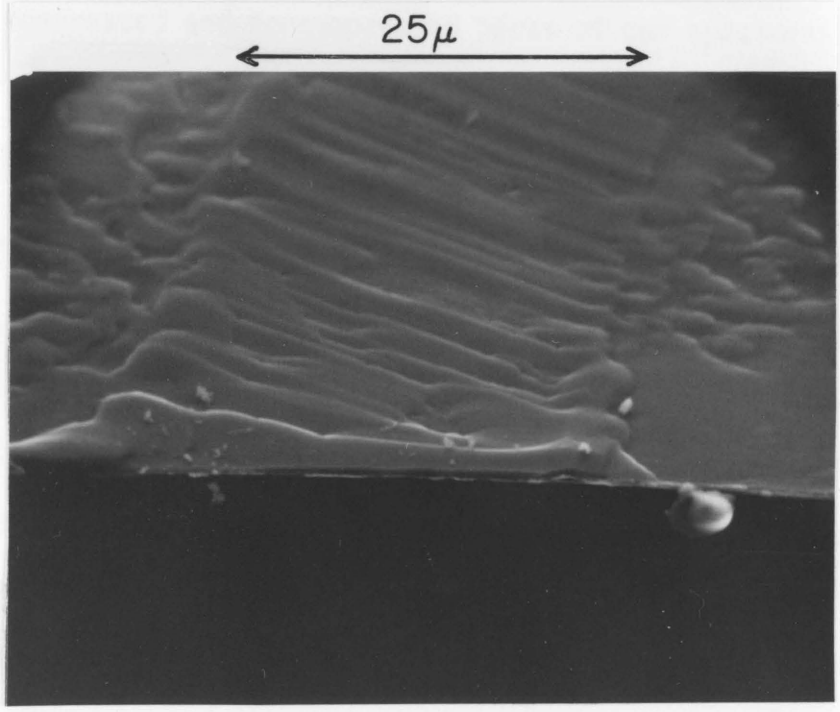
25μ

in regions where there was least amount of pressure. On the other hand, dissolution of substrate Si must have been dominant in regions of high pressure.

These results can be explained by considering the atomic volume of Si in its crystalline form (20.2Å^3) and its partial molar volume in Al (14.4Å^3) calculated from its apparent atomic diameter in Al [44]. The compression of the sample favors dissolution, since this results in a decrease of Al lattice parameter, and decrease of volume occupied by Si atoms. In fact, the solubility of Si in Al due to PV-work can be estimated to be 0.005-0.05% at 10-100 atu pressures, respectively, in stressed regions of Al. Alternately, tension should favor precipitation of Si because this results in formation of a more voluminous phase and relaxation of the lattice parameter of Al to the higher value in its pure state. The concentration gradient that thus develops between compressed and noncompressed parts of our specimens explains transport of Si. Estimates of the amount of Si transported agree with experimentally observed growth dimensions.

C. Conclusion

The mechanical stress as a driving force in the transport and growth of Si epitaxial structures in Al films was investigated. It was shown that mechanical stresses are important and effective in the growth of these structures. The stresses necessary to affect growth can be only a fraction of that necessary to cause plastic deformation of Al. Such stresses develop during thermal cycling of Si substrate Al film structures.

APPENDIX 1

The intensity of the X-ray fluorescence obtained from an element in a homogeneous mixture or alloy is given by its weight fraction, the radiation intensity in its pure state, and a series of correction factors. The composite correction factor (F) was first worked out by Duncumb [85] and Reed [86]. It can be expressed as a product of three factors: absorption factor (A) which corrects for the absorption of the host matrix elements; atomic number factor (Z) which takes into account the mean stopping power (S) of the substance, and electron backscatter factor (R) of the surface, both functions of the atomic number; fluorescence factor (C) which takes into account excitation of the continuum and characteristic fluorescence.

In the case of Al-Si, the absorption factor is expected to make the largest contribution since $Al_{K\alpha}$ is close to $Si_{K\alpha}$ line and longer than the latter. The atomic number effects are small, since the atomic numbers differ only by unity; hence, the electron capture cross sections are similar in magnitude.

The following values were calculated for the above mentioned factors for the case 1% Si-Al solution, 52.5^{o} takeoff angle (position of the diffracting crystal with respect to the plane of the specimen) and 10 keV beam voltage.

$$A = 1.344$$
$$R = 1.043$$
$$S = 1.016$$
$$Z = R \times S - 1.0596$$
$$C = 1.005$$
$$F = A \times Z \times C = 1.44$$

REFERENCES

1. G. L. Schnable, R. S. Keen, Proc. IEEE 57, 1570 (1969).
2. P. A. Totta, R. P. Sopher, IBM J. Res. Dev. 13, 226 (1969).
3. A. Y. C. Yu, C. A. Mead, Solid St. Elec. 13, 97 (1970).
4. J. R. Black, Ohmic Contacts to Semiconductors (Electrochem. Soc. Inc.) p. 311.
5. G. S. Prokop, R. R. Joseph, J. Appl. Phys. 43, 2595 (1972).
6. J. E. Lawrence, M. S. Khidr, IEEE 8th Reliability Phys. Symposium (1970), p. 285. See also 6th and 7th Ann. Rel. Phys. Symp. (1968, 1969, respectively, for various reports on the subject.)
7. M. Hansen, Constitution of Binary Alloys (McGraw Hill Publ. Co., 1958), p. 132.
8. J. O. McCaldin, H. Sankur, Appl. Phys. Lett. 20, 171 (1972).
9. H. Sankur, J. O. McCaldin, J. Devaney, Appl. Phys. Lett. 22, 64 (1973).
10. T. M. Reith, J. D. Schick, Appl. Phys. Lett. 25, 524 (1974).
11. J. Basterfield, J. M. Shannon, A. Gill, Solid St. Elec. 18, 290 (1975).
12. J. M. Caywood, Met. Trans. 4, 735 (1973).
13. J. M. Caywood, A. M. Fern, J. O. McCaldin, G. Ottaviani, Appl. Phys. Lett. 20, 326 (1972).
14. J. O. McCaldin, H. Sankur, Appl. Phys. Lett. 19, 527 (1971).
15. G. Ottaviani, D. Sigurd, V. Marrello, J. W. Mayer, J. O. McCaldin, J. Appl. Phys. 45, 1730 (1974); and D. Sigurd, G. Ottaviani, H. J. Arnal, J. W. Mayer, to be published in J. Applied Physics.
16. A. Hiraki, E. Lugujjo, J. W. Mayer, J. Appl. Phys. 43, 3643 (1972).

17. H. Sankur, J. O. McCaldin, J. Electrochem. Soc. 112, 565 (1975).

18. A. Hiraki, M. A. Nicolet, J. W. Mayer, Appl. Phys. Lett. 18, 178 (1971).

19. T. Oki, Y. Ogawa, Y. Fujiki, Jap. J. Appl. Phys. 8, 1056 (1969).

20. J. R. Bosnell, U. C. Voisey, Thin Solid Films 6, 161 (1970).

21. S. Herd, P. Chandhare, M. H. Brodsky, J. Non-Crys. Solids 7, 309 (1972).

22. D. H. Lee, R. R. Hart, O. J. Marsh, Appl. Phys. Lett. 20, 73 (1972).

23. U. Koster, Acta Metall. 20, 1861 (1972).

24. J. F. Ziegler, J. W. Mayer, C. J. Kircher, K. N. Tu, J. Appl. Phys. 44, 358 (1973).

25. H. Kräutle, M. A. Nicolet, J. W. Mayer, J. Appl. Phys. 45, 3304 (1974).

26. H. Kräutle, M. A. Nicolet, J. W. Mayer, Phys. St. Sol.(a) 20, K33 (1973).

27. R. W. Bower, J. W. Mayer, Appl. Phys. Lett. 20, 359 (1972).

28. W. D. Buckley, S. C. Moss, Solid St. Elec. 15, 1331 (1972).

29. M. Beguwala, C. R. Crowell, J. Appl. Phys. 45, 2792 (1974).

30. R. W. Bower, Appl. Phys. Lett. 23, 99 (1973).

31. A. K. Sinha, J. M. Poate, Appl. Phys. Lett. 23, 666 (1973).

32. J. Gyulai, J. W. Mayer, V. Rodriguez, A. Y. C. Yu, H. J. Gopen, J. Appl. Phys. 42, 3578 (1971).

33. B. R. Pruniaux, J. Appl. Phys. 42, 3575 (1971).

34. J. Gilles, J. Van Cakenberghe, Nature 182, 862 (1958).

35. A. Vecht, J. Vac. Sci. Tech. 6, 773 (1969).

36. V. Marrello, J. M. Caywood, J. W. Mayer, M. A. Nicolet, Phys. St. Sol.(a) 13 (1972).

37. C. Canali, J. W. Mayer, G. Ottaviani, D. Sigurd, W. v.d. Weg, Appl. Phys. Lett. 25, 3 (1974).

38. K. N. Tu, W. K. Chu, J. W. Mayer, to be published.

39. C. Canali, S. U. Campisano, S. S. Lau, Z. L. Liau, J. W. Mayer, to be published.

40. A. M. Fern, J. O. McCaldin, Proc. IEEE 60, 1018 (1972).

41. G. Ottaviani, V. Marrello, J. W. Mayer, M. A. Nicolet, J. M. Caywood, Appl. Phys. Lett. 20, 323 (1972).

42. V. Marrello, T. A. McMath, J. W. Mayer, J. C. Fowler, Nuc. Inst. Meth. 108, 93 (1973).

43. G.J. v.Gurp, J. Appl. Phys. 44, 2040 (1973).

44. H. J. Axon, W. H. Rothery, Proc. Roy. Soc. A193, 1 (1948).

45. E. H. Dix, A. C. Heath, Trans. AIME 78, 164 (1928).

46. V. M. Glazov, Izv. Akad. Nauk, SSSR Otd. Tekhn. Nauk, Met. i, Toplivo 4, 39 (1961).

47. E. Kovacs, C. Cstenyi, C. R. Vassel, I. Kovacs, Ph. St. Sd. 17, K123 (1966).

48. H.W.L. Philips, J. Inst. of Metals 72, 158 (1946).

49. G. Tammann, W. Oelsen, Z. anorg. Chem. 186, 285 (1930).

50. S. T. Rostovtsev, S. I. Khitrik, B. I. Emlin, M. I. Gasik, A. I. Dobrebniyak, Izv. Vyssh. Ucheb. Zaved. Chern. Met. 14, 61 (1971); Chem. Abstr. 74, #147077S.

51. R. F. Mehl, F. N. Rhines, K. A. Steinem, Metals and Alloys 13, 41 (1941).

52. W. G. Fricke, Jr., ASM Trans. Quarterly 58, 421 (1965).

53. A. Beerwald, Z. Elektrochem. v. Ang. Phys. Chem. 45, 789 (1939).

54. W. Roth, Metallwiss. v. Technik. 14, 979 (1960).

55. H. R. Freche, AIME Trans. 122, 324 (1936).

56. H. Bückle, Z. Elecktrotech. 49, 238 (1943).

57. P. L. Ferraglio, C. D'Antonio, Thin Solid Films 1, 499 (1967).

58. H. G. v. Bueren, Imperfections in Crystals (North-Holland Publ. Co., Amsterdam, 1962).

59. T. E. Volin, K. H. Lie, R. W. Baluffi, Acta. Metall. 19, 263 (1971).

60. R. E. Mistler, R. L. Coble, J. Appl. Phys. 45, 1507 (1974).

61. C. Pansuri, T. Federighi, Phil. Mag. 3, 1223 (1958).

62. P. L. Castro, J. F. Campbell, Ohmic Contacts to Semiconductors, (Elec. Chem. Soc. Inc.) p. 332.

63. B. Ghate, J. C. Blair, IEEE Trans. Parts. Hyb. Pack.___, 134 (1971).

64. M. Hagaki, B. C. Giessen, N. J. Grant, Trans. ASM 61, 330 (1968).

65. E. Ozawa, H. Kimura, Acta Metall. 18, 995 (1970).

66. H. S. Rosenbaum, D. Turnbull, Acta Metall. 6, 653 (1958) and 7, 664 (1959).

67. T. M. Donovan, E. J. Ashley, W. E. Spicer, Phys. Lett. A32, 85 (1970).

68. R. H. Saul, D. D. Roccasecca, J. Appl. Phys. 44, 1983 (1973).

69. H. J. Kim, J. Electrochem. Soc. 119, 1394 (1972).

70. D. K. Schroder, R. A. Wickstrom, P. Rai-Choudhury, Appl. Phys. Lett. 23, 66 (1973).

71. J. M. Shaw, J. A. Amick, RCA Rev. 31, 306 (1970).

72. I. H. Khan, J. Appl. Phys. 44, 14 (1973).

73. F. A. Trumbore, Bell Syst. Tech. J. 39, 205 (1960).

74. K. L. Dunning et al., Thin Solid Films 19, 145 (1973).

75. K. L. Dunning, H. L. Hughes, IEEE Trans. Nucl. Sci. 19, 243 (1972).

76. M. Tannenbaum, N. B. Hannay, Semiconductors (Reinhold, New York, 1959).

77. J. H. Broghy et al., Structures and Properties of Materials 12, (Wiley, New York, 1964).

78. R. A. Landisse, J. R. Carruthers, K. A. Jackson, Ann. Rev. Mat. Sci. (1971).

79. L. R. Dawson, Progress in Solid State Chemistry 7 (Pergamon Press), p. 117.

80. K. H. Henisch, Crystal Growth in Gels (Pennsylvania State University Press, Univ. Park, 1970).

81. L. E. Katz, J. Electrochem. Soc. 121, 969 (1974).

82. K. V. Ravi, C. J. Varher, C. E. Volk, J. Electrochem. Soc. 120, 533 (1973).

83. R. A. Swalin, J. Phys. Chem. Sol. 18, 290 (1961).

84. J. S. Best, J. O. McCaldin, "Si-Al interface shapes developed during heating of integrated circuits", to be published.

85. D. Duncumb, P. K. Shields, Brit. J. Appl. Phys. 14, 617 (1963).

86. S.J.B. Reed, Brit. J. Appl. Phys. 16, 713 (1965).

PART II

INVESTIGATIONS ON THE INTERFACE EFFECTS IN Si-Au AND ON THE PHASE DIAGRAM OF Si-Au-Cu

1. INTRODUCTION

A. General

The equilibrium phase diagram of Au-Si is a simple binary eutectic system [1]. The equilibrium phases studied by various investigators [2-5] indicates that the system was characterized by a deep-lying eutectic temperature--at 48% and 38% of the melting points of Au and Si, respectively--and extremely limited solid solubilities. Some of the more recent investigations pointed out the underlying complexity of this system: A number of metastable compound phases have been obtained under quenching [9-11], splat cooling [6-8], sputtering [12], low temperature treatment of Au films in oxidizing atmosphere [13]. The sluggish nature of the crystallization kinetics and the stability of the liquid at low temperatures was interpreted as an indication of compound-like association of the Au and Si atoms in liquid phase [11,14,15]. This behavior was exploited by D.Turnbull [16] to induce glass transition in this system upon addition of Ge.

Some of the recent investigations on this system have been motivated because of the utilization of Au in semiconductor device technology. Thin Au films are used as metallization in integrated circuits and in microwave power devices, beam lead devices, and as eutectic preform to attach Si chips to packages.

The extensive use of Au metallizations in microwave power devices and in integrated circuits is due to its high conductivity, low failure rate due to electromigration [17], chemical stability with respect to corrosion. Recent findings, however, suggest that halogenic contaminants,

humidity and potential bias, lead to catastrophic failure of semiconductor devices due to electrochemical corrosion [18] of the Au metallizations.

A different catastrophic failure of devices is caused by Si-Au interface reactions. In devices, either an oxide layer separates Si and Au films, or refractory metal layers are deposited between Au and Si to serve such purposes as providing low resistivity, reliable ohmic contacts (Pt or Pd), adhesion to the substrate (Ti), and as interdiffusion barriers (W,Mo,Ti). Extensive dissolution of Si and migration of it in Au takes place at low temperatures when Au and Si come in contact due to mechanical damage to the intermediate layers or chemical reactions in the diffusion barriers [19]. The localized pitting that results in the Si surface may cause shorts between thin planar diffused layers. In the present investigation the effect of interface conditions on the dissolution reaction of Si in Au has been studied, and the morphology of the dissolution pattern characterized.

The relatively high rate of diffusion of Si in thin Au films at temperatures as low as 150^{o}C [20] makes the latter [11] a suitable medium for the transport and growth of thin semiconductor layers (as explained in Part I, 1C). Therefore, attempts were made in the present investigation to measure solubility and diffusivity of Si in Au films.

B. Interface Effects in the Dissolution of Si into Thin Au Films

The interface conditions at Si-Au interface had been shown to affect the dissolution reaction of Si into Au films [21,22]. In the present investigation an extensive qualitative evaluation of this effect is investigated.

The dissolution of Si was extensive in the presence of a sink for Si. The sink was a layer of Pd, away from the Si-Au interface. Pd reacted with and stabilized Si atoms that migrated to the surface of the Au film, as will be clarified further on.

The present investigation showed that dissolution was nonuniform across the plane of the Si surface. Isolated pits and trenches formed on the Si surface, corresponding to dissolution regions. The dissolution behavior showed dependence on the Si crystal orientation as well as on the presence of thin metal films at the Si-Au interface [23].

These findings stress the role the surface contaminants--in the form of oxide films and organic and inorganic residues from polishing or cleaning processes--play in affecting the surface reactions. The non-uniformity in microscale of thin film interactions and surface reactions may be more commonplace than realized by some of the previous investigators who utilized averaging measurement techniques, such as X-ray diffraction, He^+ backscattering, Auger or mass spectrographic analysis coupled with sputter etching. Localized chemical analysis, which has been possible with electron microprobe and can also be accomplished with more developed variations of the above-mentioned techniques, is necessary in order to fully characterize these reactions.

In the present investigation, solubility and diffusivity of Si in Au films were also studied by means of the electron microprobe analysis. However, quantitative data were not obtained due to limitations of the analysis techniques.

C. Investigation on Si-Au-Cu Phase Diagram

The solubility of Si in Au appears to be below the detectability of some of the presently available techniques. X-ray diffraction analysis of lattice parameter [24] of Au-Si alloys, and microprobe analysis of thin film specimens [23] failed to provide quantitative solubility data. The present experiments established an upper limit for solubility as explained in detail in Section 2A, Part II.

Cu-Si system, on the other hand, is known to form several intermetallic compounds and an extensive solid solution at Cu-rich end of the diagram [25].

The investigation of Si solubility in Cu-Au alloys was undertaken in view of the fact that Cu and Au form continuous solid solutions [26]. Therefore Si-Cu-Au were expected to form a ternary solid solution continuous from Cu to Au rich end of the diagram. The variation of Si solubility with Au in the ternary solution could be extrapolated to the Au rich side, yielding information on Si solubility in Si-Au binary system.

The latter information will be useful to analyze the kinetics of Si transport in thin films: The total amount of Si transported, or the permeation of Si through Au films can be measured experimentally, under suitable conditions. The rate of permeation, however, is given by the product of diffusivity, the kinetic term, and solubility, in addition to geometrical factors.

The information on kinetics is important in predicting the reliability of semiconductor devices in regard to failure due to Si dissolution and in controlling growth of epitaxial layers in solid state.

Investigation of Si-Au-Cu may also prove worthwhile because of the potential use of Cu-Au films as a medium for transport and growth of

semiconductor structures in solid state. Addition of Cu to Au enhances Si solubility, and may thus favor bulk diffusion of Si in thin Cu-Au films over diffusion of Si through structural defects, as appears to be the mechanism of transport in thin Au films. The latter condition may thus induce a slower diffusion of Si and smoother diffusion front, hence more uniform growth of semiconductor layers in solid state.

In the present investigation the ternary solid solution at Cu-Au rich end of the phase diagram was studied. The analysis techniques used were X-ray powder diffraction and microscopic analysis of bulk specimens. The boundary of the ternary phase or the maximum Si solubility in Cu-Au showed decrease of Si concentration as Au content of the alloy increased, with the exception of an increase of Si concentration between 45-65% Au. The Si solubility could not be extrapolated to high Au concentrations of the ternary alloy, because of the non-monotonic behavior of the boundary and because the solubility fell to very small values at Au concentrations above 75%.

2. INTERFACE EFFECTS IN THE DISSOLUTION OF Si INTO THIN Au FILMS

In the present investigation of Si dissolution in Au, the solubility of Si and the detectability limit of Si in Au had to be investigated. Previous investigations [24] by others had indicated an upper limit of 0.1 atomic percent for solubility.

Solubility of Si in Au

A. Sample Preparation and Analysis

The samples used in solubility experiments consisted of crystalline Si wafers or polished vitreous carbon as substrates and 1 micron thick Au film evaporated onto these. Amorphous Si was vapor deposited onto a portion of the C substrates before Au evaporation.

The Si substrates were cleaned in organic solvents, rinsed, and dipped briefly in HF before vapor deposition of the Au film. The evaporations were done in a vacuum system equipped with a 3 crucible electron gun system, at pressures of 10^{-6}-10^{-7}torr. The samples were annealed in vacuo at various subeutectic temperatures for several hours, and then allowed to cool rapidly. The analysis was performed with an electron microprobe tuned to detect SiKα radiation.

The electron beam energy was of such a magnitude that it did not reach the Si substrate. However, in specimens with C as substrate, the beam penetrated the Au film to reach the C-Au interface, away from the vapor deposited amorphous Si, to probe for Si in solution and Si that may have precipitated on the C substrate during cooling.

Thus Au films were probed for Si that diffused in the vertical direction in samples with Si substrates, and for Si that diffused in the lateral directions in samples with C/Si substrates.

B. Results and Discussion

The electron microprobe analysis performed with a finely focussed beam indicated that solubility was too low to be detected by this method. An upper limit for solubility--0.02%--was set by the interference of Au (M_{IV}-N_{III}) transition line. This resolution of a detector necessary to separate the main source of noise from the signal should be better than 50 eV. Solid state detectors made with Li diffused high purity Ge can give such a good resolution, if the noise of the electronic circuitry is also reduced by use of optical feedback amplifiers.

The resolution can also be improved by interposing a narrow slit between the sample-source of X-rays and the diffracting crystal, in order to reduce the divergence of the incoming radiation. However, the increase of signal to noise ratio at SiKα line due to improvement

of the instrument will not be significant in view of the fact that noise from many lines of the Au matrix is as high as to constitute 0.3% of the signal from pure Si at 10 keV beam energy.

The sensitivity for detection of Si in Au can be increased if radiation from the Si isotopes, produced by neutron activation, is measured. $_{14}Si^{31}$ with a lifetime of 157 min is the only available isotope for Si. The background noise due to Au isotopes is likely to be small. The γ-ray emitted by $_{79}Au^{194}$, closest in energy to the Si isotope line, is small in intensity and these two lines can be resolved by good nuclear particle detectors.

Higher sensitivity can be achieved if the sample is subjected to secondary ion mass spectroscopy analysis (as explained in Part I, 4C). Nonuniformity in sputtering rate or profile will not be important in this case, since total Si concentration will be analyzed.

Interface Effects

C. Sample preparation and analysis

The impossibility of detecting Si in the pure Au films necessitated the use of a sink for Si. The sink consisted of a Pd overlay on the Au film which reacted with and stabilized Si which diffused through the Au film (Fig. 1). Si that thus accumulated as silicide by reacting with Pd was available for microprobe analysis. The amount of this corresponded to the Si that dissolved and migrated through the Au film.

The typical samples were prepared with chemically polished Si wafers (p-type, .1-10 -cm) as substrate with their surface plane normals

Fig. 1

Cross section of a specimen schematized to illustrate the experiment. Note that vertical dimensions are not drawn to scale.

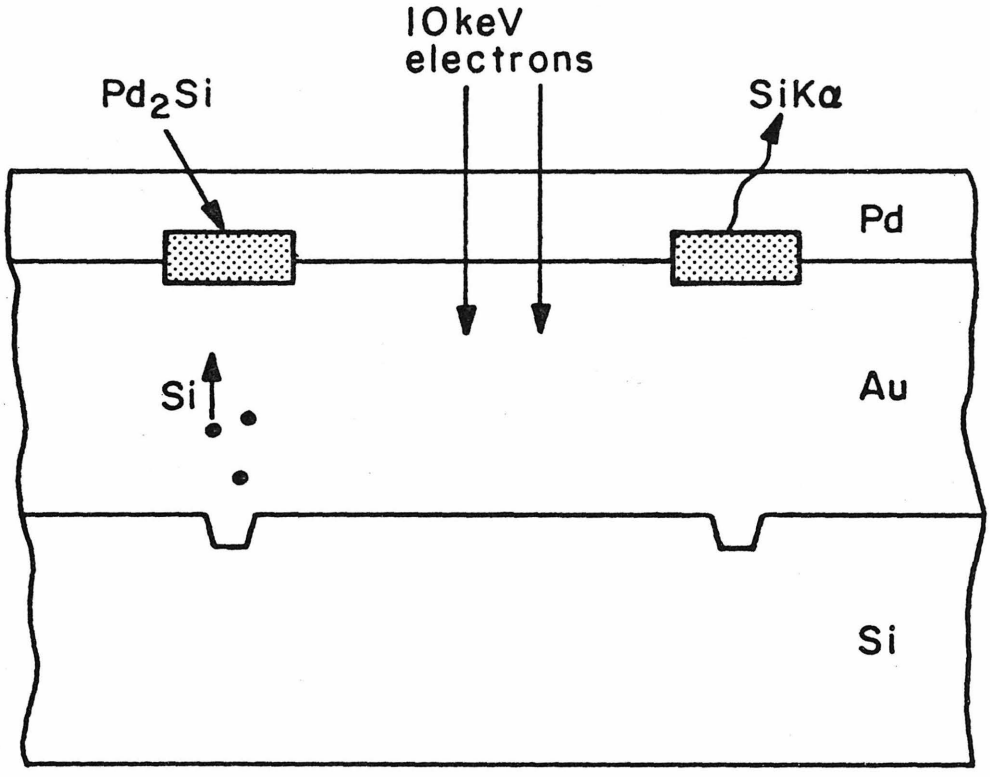
10keV
electrons
Pd_2Si
SiKα
Pd
Au
Si
Si

aligned with (111), (110) or 100 directions. Thermally oxidized Si wafers were used as support for evaporated amorphous Si substrates. Au film, 1μ in thickness from a 99.9999 purity source and 600Å thick Pd film from a 99.9 source were evaporated on these substrates. All evaporation, including Si layer, were done sequentially from a 3 crucible electron gun, at a pressure of 10^{-6}-10^{-7}torr. A class of specimens had 200Å Pd film between Au and Si substrate.

These specimens were annealed at 220°C in a tube furnace provided with a vacuum pump facility. The pressure during annealing was kept below 10^{-5}torr by means of an oil diffusion,Ti sublimation and cryogenic pumps. The samples were stored in a desiccator under vacuum, to avoid formation of oxides.

A few specimens were prepared by omitting Pd overlay deposition. These were annealed in wet N_2, thus substituting oxidizing agents for Pd as sink for Si.

The samples were then subjected to electron microprobe analysis in scanning mode--as explained in Part I, 3A. The Pd and Pd_2Si layers were removed in boiling (NHO_3+ H_2SO_4) mixture, which did not attack Au film, and the Au film was removed in KI + I_2 solution, to prepare the Si surface for SEM study.

Quantitative data about Pd_2Si growth were obtained as a function of growth time. The latter electron microprobe analysis was performed with a defocused beam, to average Si signal from a region approximately 50μ in diameter.

D. Results

Pd-Au interdiffusion was studied with He^+ backscattering measurements and found to be negligible at the annealing conditions of the present experiment, in agreement with literature data [27]. The above mentioned condition was necessary in order for the Pd layer to be a stationary sink for Si on one side of the Au film. If Au and Pd were to interdiffuse regionally or form a solid solution in a brief period of time, the Pd near Si-Au interface would have affected dissolution behavior of Si, as will be clarified further on. On the other hand, formation of Pd_2Si at the top interface stopped any further Pd-Au interdiffusion.

The main results of the present investigation were the nonuniform nature of Si dissolution and the dependence of the latter on substrate crystalline orientation. In general, the dissolution pattern of the substrate consisted of 1-5μ wide trenches on the Si surface, which formed closed curves from the top view. This pattern was essentially replicated in the Au and Pd films as a result of migration through and compound formation of Si in metal films.

Microprobe analysis of the silicide growth gave an indication about the above mentioned results: Figs. 2a, 3-6 are micrographs of the silicide compound as exhibited by the microprobe in scanning mode. The light areas correspond to places where Si is present at the top surface of Au in the form of Pd_2Si. These could also be identified by optical observations as seen in Fig. 2b. A comparison of Figs. 2a, 3-5 shows that the distance between the curved band or line shaped

Fig. 2

A section of the complete specimen (a) as exhibited by the electron microprobe tuned to detect SiK_α fluorescence. Si in the Pd_2Si appears as white in this photograph. (b) SEM photograph of the same section of the specimen after the microprobe analysis. (c) SEM photograph of the same area of the Si surface after removal of all metal and silicide. The substrate was <111> Si.

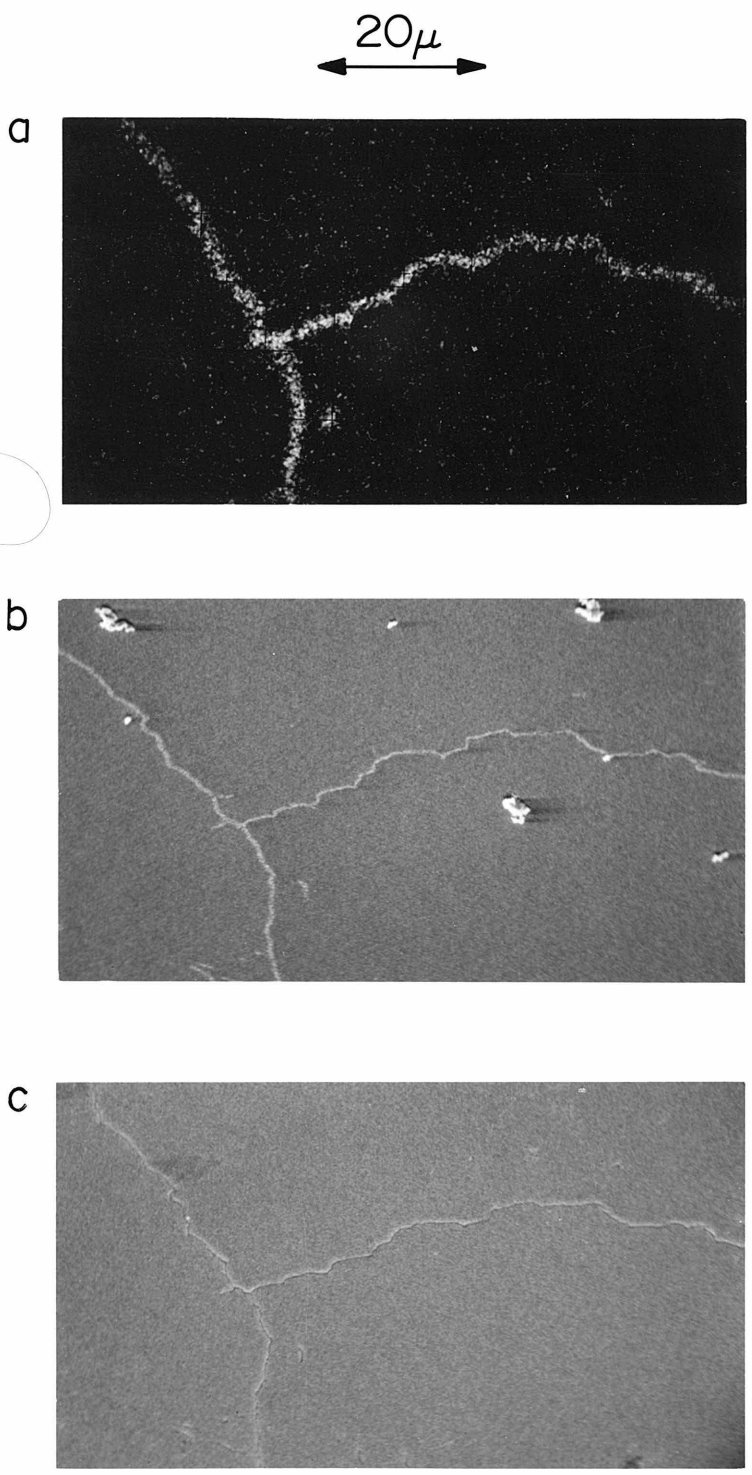
20μ
a
b
c

Fig. 3

Micrograph obtained in the microprobe analysis, showing another location of specimen in Fig. 2 where white areas represent silicide within the metallization.

Fig. 4

Microprobe photograph of a specimen with (100) Si substrate. The specimen was annealed at 220^{o}C for 1 hour.

50μ

10μ

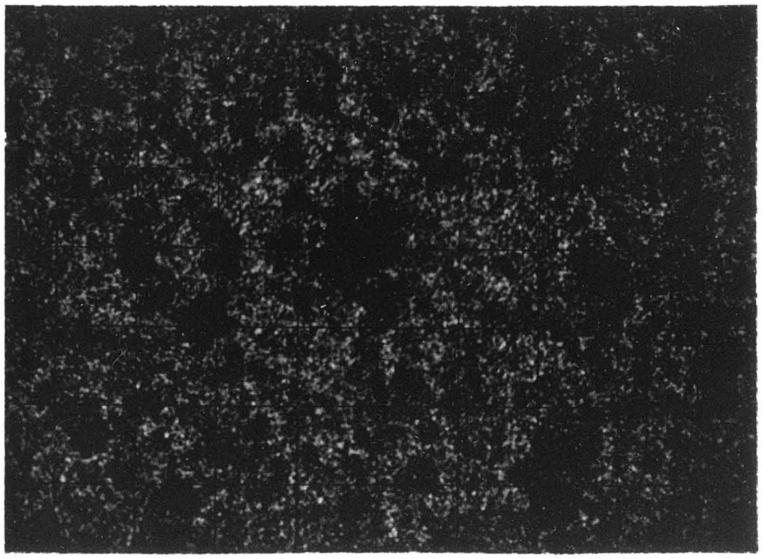

Fig. 5

Microprobe photograph of a specimen with (110) Si substrate.

Fig. 6

Microprobe photograph of a specimen with <111> Si substrate and a thin Pd layer deposited between Au film and Si. Note the increased density of silicide clusters compared to Fig. 2.

20μ

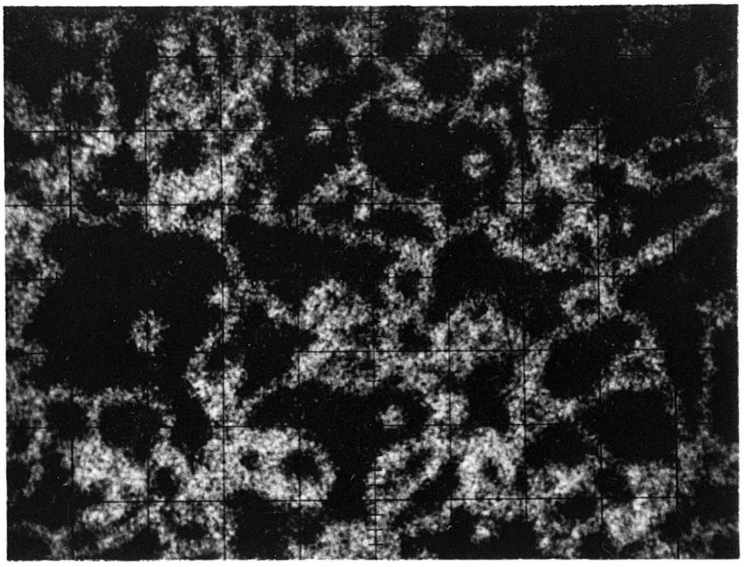

10μ

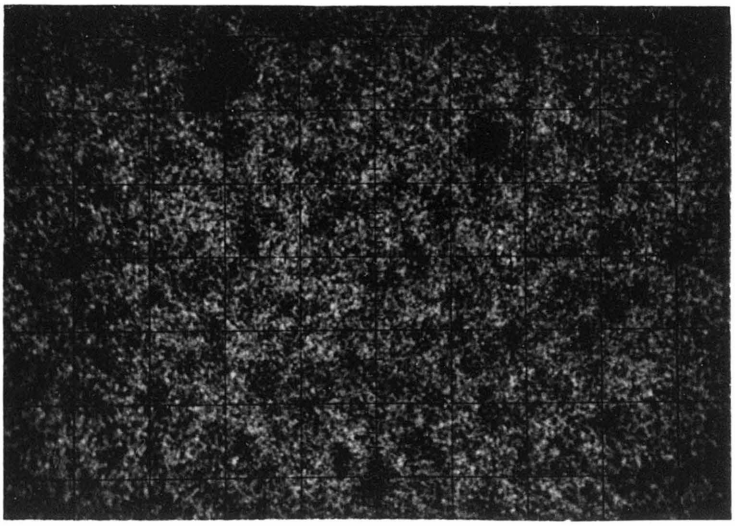

growth structures in samples with (111) oriented substrates is large (30-100μ) Figs. 2a, 3 compared to that in 110 oriented substrates (5-20μ) Fig. 5 and 100 oriented substrates (5-10μ) Fig. 4. The areas enclosed by the growth features do not contain any silicide.

Actually, the samples with (111) oriented substrates showed a variety of silicide growth features: jagged lines (Fig. 3), short jagged broken lines, and dense array of points within an area enclosed by a continuous line. The silicide bandwidth as measured from the top surface was on the order of 5-10μ. This width increased with time, until the surface was totally covered by a silicide layer in the case of samples with 100 or 110 oriented Si substrates.

The above-described topographical features were observed to be replicated in the Au film and Si surface, when the Pd and both Pd and Au were removed, respectively. SEM observation revealed depressions on the Au film surface (Fig. 7) corresponding to location of silicide growth. The depressions formed due to the volumetric changes accompanying compound growth. The optical surface features on the Pd film were also due to surface deformations in addition to color change when the compound growth reached the surface.

SEM analysis of the Si surface showed that pits (Fig.8); channels in the form of canyons 0.1-0.3μ deep and 1-5μ wide, continuous (Fig.9) or consisting of rectangular pits (Figs.10,11) had formed on the surface. Comparison of Figs.2a,2c indicates that dissolution trenches and silicide growth features occur on the same vertical plane. Au atoms migrated into and filled the trenches without any loss of adhesion of the film (Fig.12). The raised structures, as observed on the side of the Au film in contact with

Fig. 7

SEM picture of the Au surface of a specimen that was annealed in an oxidizing atmosphere. SiO_2 growth structures that had formed along the channels were chemically removed. Note that considerable plastic flow must occur in the Au film to accommodate the SiO_2 growth structures on the Au surface.

Fig. 8

Close-up SEM view of dissolution pits on the Si surface. The annealing time was 9 hr, during which all Pd was transformed into the silicide. Note the faceted walls of the pits.

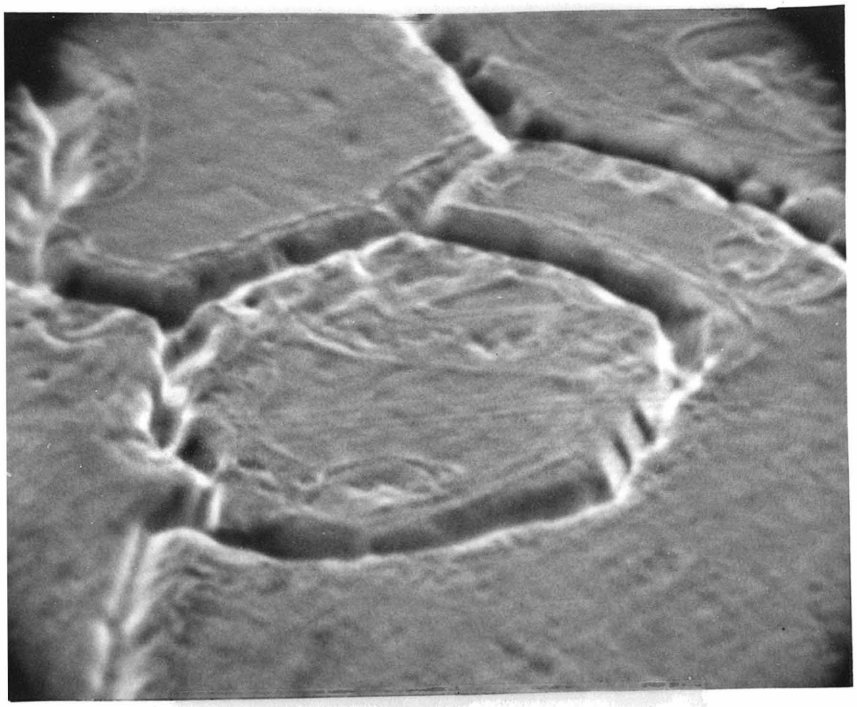

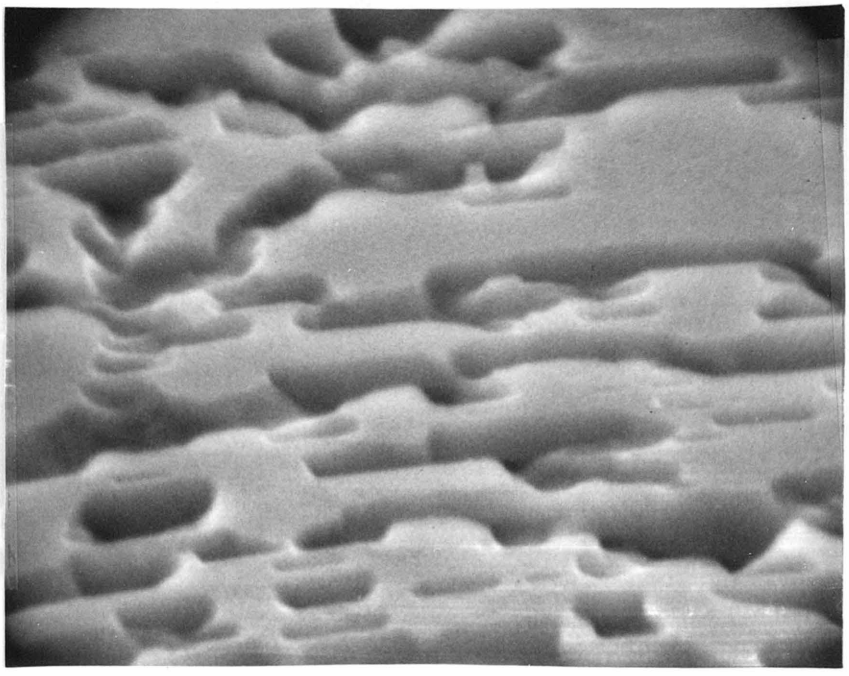
2μ

Fig. 9

Top and edge SEM view of a dissolution trench in (111) Si surface.

Fig. 10

SEM picture of the dissolution pattern consisting of elongated pits aligned in curved lines. The substrate was 100 Si. The metal films were removed prior to SEM analysis.

1μ

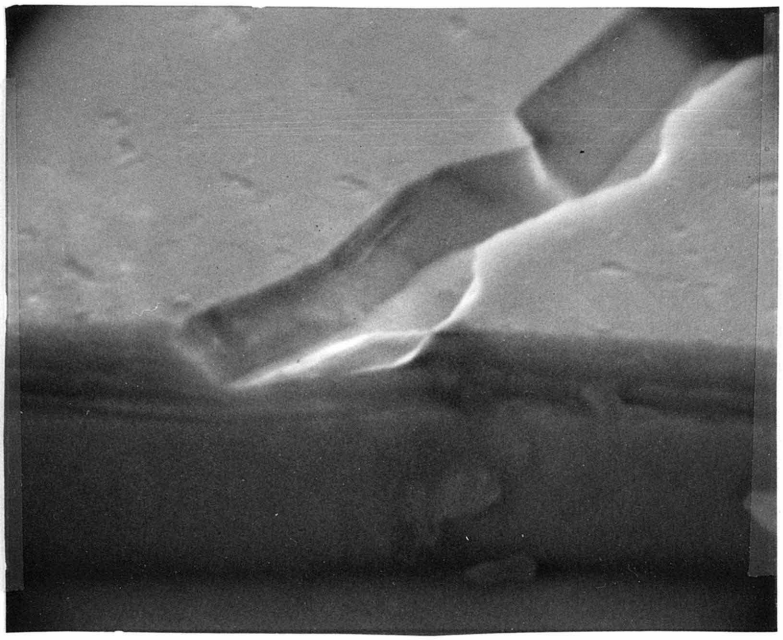

20μ

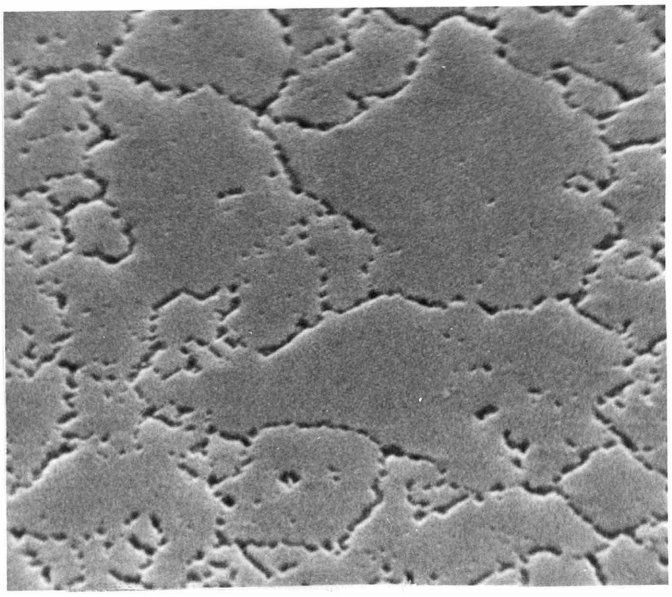

Fig. 11

SEM picture of the dissolution pattern in a 100 Si substrate. Note that pit walls are parallel to each other, a fact that reflects substrate crystallinity.

Fig. 12

The back side of the metallization after removal of the Si substrate. The raised features correspond to trenches in the <111> Si substrate, and the faceted nature of them reflect the crystalline nature of the substrate.

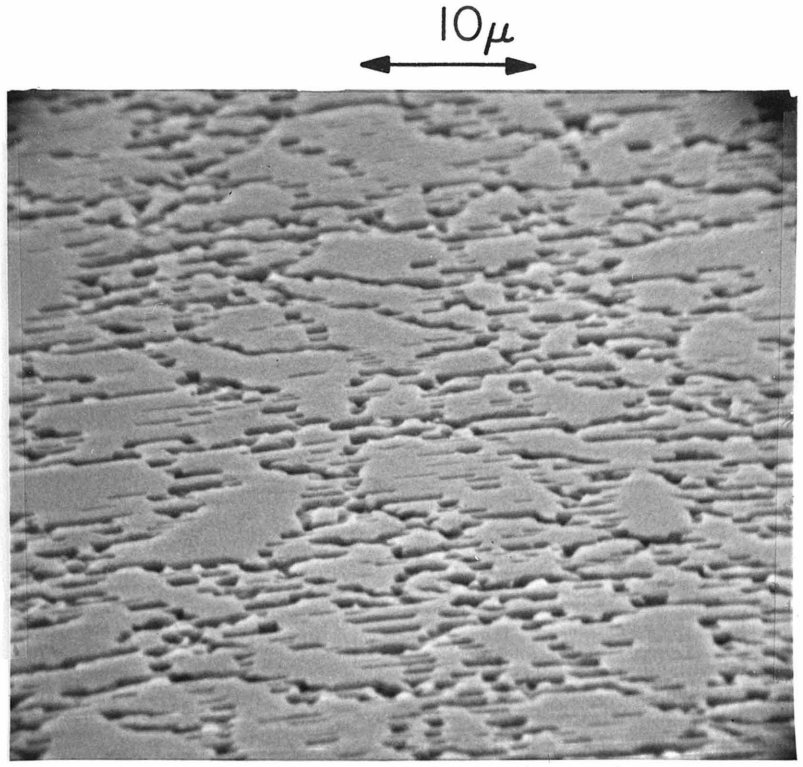
10μ

Si substrate show that the trench walls often exhibited crystal faceting.

The dissolution picture changed dramatically when a thin Pd or Si underlay was evaporated onto crystalline substrates. The silicide formation on the top surface occurred in a much denser array of points, lines, bands (Fig. 6). The facilitated dissolution occurred independent of Pd underlay thickness, which was varied between 100-1000Å.

Essentially, results similar to all the above-described were obtained when the sink layer Pd was substituted with oxide forming agents. Microprobe, chemical and SEM analysis indicated that formation of SiO_2 on the surface and of the dissolution trenches on the Si surface were similarly nonuniform and dependent on substrate crystalline orientation and interface conditions in these specimens.

E. Discussion

The localized nature of thin film reactions is probably due to the effect of thin oxide or chemical residues from polishing or wafer cleaning on the Si surface: heavy metal cations in chemical etchants and rinse solvents are found to deposit irreversibly on semiconductor surfaces in metallic form [28]. In the case of Si, the large difference in oxidation potentials between Si and these metals facilitates adsorption of monolayers of Au, Cu, Cr and smaller amounts of Fe, Sb, Zn, Mn from etch solutions contaminated with these elements in ppb levels. These results have been obtained in recent investigations using radioactive tracer techniques [29]. Similarly, halogen and acetate ions are found to be adsorbed or to form complexes with oxygen and Si

on the wafer surface [30].

Organic residues, on the other hand, may prevent desorptive cleaning of inorganic impurities because of their hydrophobicity.

The "dirt" layer can hinder chemical reaction at the interface, by preventing Au and Si from coming into intimate contact. Au is not a chemically active element like Al and some refractory metals which are known to react with or destroy the coherency of the "dirt" layer. Thus, in the case of Au-Si layer, dissolution reaction may proceed at weak spots, cracks, pinholes in the dirt layer.

In the present experiments inorganic or organic impurities did not play a major role, since the wafers were cleaned with organic solvents and rinsed thoroughly in deionized water before being loaded into the evaporator. This procedure is known to reduce the adsorbate concentration drastically. Native oxide, which grows on the bare surface of Si when the latter comes in contact with air, is more likely to act as a barrier to Au-Si interaction in the present experiments.

The observed difference in dissolution behavior between substrates with (111) and other orientations supports the latter hypothesis. The higher atomic density of 111 planes should produce a more coherent and thicker oxide [31]. The surface oxide was also observed to affect similarly reaction between Si and W films [32].

A demonstration of the above mentioned effect was provided by the experiments where Si wafer was boiled in HNO_3 to grow a thin oxide layer before the vapor deposition process. No reaction occurred in these specimens under prolonged treatment.

The effect of Pd underlay in facilitating Si dissolution can be explained in terms of the greater chemical reactivity of this element with respect to Au. Pd may getter some impurities, although it cannot reduce SiO_2, or may disrupt the coherency of the adsorbed layer or of the thin oxide layer when it reacts with Si to form the silicide layer at Si-Pd interface.

Pd, as sink material did not have a direct role in the dissolution behavior of Si. In fact, essentially identical results were obtained when gaseous H_2O or O_2 were substituted for Pd to form SiO_2, hence to stabilize Si on the Au surface. The effect of grains in the Au film also are not likely to produce the observed effects, since samples with different substrate crystalline orientations were processed in an identical manner and simultaneously. An experiment designed to observe the effect of Au grain size was performed when the Au film was annealed in vacuo for 3 hr at 250°C before Pd deposition. This treatment should produce considerable recrystallization of the Au film [33]; however, dissolution behavior of Si did not change.

F. Studies on Diffusion of Si in Au

The microprobe analysis of the growth rate of the silicide on the Au film did not result in quantitative data on the diffusion of Si in thin Au films. In this analysis, counts were taken of SiKα intensity, at 10 min intervals of an isothermal treatment at 220°C, with an electron beam defocused to a diameter of 50μ in a single location of a specimen. The results indicated that the amount of silicide increased monotonically with time, but the time dependence varied with the cumulative annealing time and Pd film thickness. This suggests that Si

diffusion in Au is not the limiting step in the overall reaction.

An experiment was designed to make Si diffusion the slow step in the kinetics by increasing the diffusion distance. In this analysis samples prepared by evaporating two thin strips--one of Si, the other of Pd on opposite sides of a 1μ thick Au film were annealed for different periods of time. The strips were displaced laterally from each other. Microprobe measurements indicated that silicide growth was limited to areas at and within 1μ of the geometrical union of the two strips. This suggests that texture of the Au film or thermal stresses in it may influence the diffusion of Si.

The data on the growth rate of silicide were used to obtain an estimate for Si diffusivity in Au at 220°C ($D \geq 10^{-9} cm^2/sec$). This was a lower limit, since experiments indicated that Si diffusion was not the slow step of the reaction. This estimate was obtained using permeation = diffusivity x solubility x time/diff. length , and making use of the solubility estimate obtained earlier. This estimate may be explained in terms of structural defects of the Au film or in terms of the effect of metastable compounds. Dislocations, stacking faults, grain boundaries, quenched-in excess vacancies have been observed in vapor deposited metal films. These provide paths of rapid diffusion due to lowering of the activation energy for diffusion. The increase in potential energy due to local strain as the diffusing atom exchanges place with a vacancy is less when the atomic stacking order is broken as is the case at these defect sites. A comparison with the Si-Al system (Part I, 2Bb) where the activation energies for Si diffusion in the Al film and diffusion through dislocations in Al were found to be nearly equal, suggests that activation energy for

Si diffusion in Au may be 1.0 ∓ 0.1 eV [33]. These values would qualitatively explain the room temperature diffusion of Si in Au observed by means of ESCA analysis [34].

An alternate hypothesis bases on the formation and dissociation of metastable compounds [6-14]. These may form at the interface where Au and Si come in intimate contact. In fact, A. Hiraki et al. observed some of the metastable compounds at low subeutectic temperatures in thin films deposited on Si, by means of Auger spectroscopic analysis [13]. The concentration gradient of Si that thus develops in the Au film may drive the diffusion. Si atoms are consumed at Pd-Au interface on account of the greater stability of palladium silicide with respect to Au compounds.

G. Conclusion

Dissolution of crystalline and amorphous Si into thin Au films was studied with electron microprobe and SEM analysis. Si was found to migrate through the Au film in solid state, only in isolated points or lines. The separation between dissolution locations depends on the substrate crystalline orientation and on the presence of a thin Pd layer deposited between Au and Si. The localized dissolution was attributed to the effect of the surface adsorbed impurity or native oxide layer.

Investigations on the solubility and diffusivity of Si in Au did not produce quantitative results other than estimates of upper and lower limits respectively for the two parameters.

3. INVESTIGATION OF Si-Au-Cu TERNARY SYSTEM AT LOW Si CONCENTRATIONS

A. Sample Preparation and Analysis

Sample alloys were prepared from 99.9999% purity Au pellets, 99.999% purity Cu, and 10Ω cm resistivity semiconductor-grade crystalline Si, each weighed to greater than 0.1% accuracy. The constituents were cleaned with organic solvents, dried before being melted by means of an RF furnace. The oxide skins on Cu and Si were etched in HCL and HF respectively before melting. The alloying took place in a quartz tube in which dry low pressure Ar was circulating. The molten alloy was cooled at the approximate rate of 100^{o}C/sec by immersing the quartz tube in water. Reweighing the alloy indicated that no measurable loss of material had occurred during melting. Micrographic and powder diffraction pattern analysis indicated that Cu-Au alloys prepared according to the above procedure were homogeneous.

The alloys were annealed at 349 ∓ 1^{o}C for 192 hr in a 4 mm quartz tube, one end of which was sealed. The latter was inserted in a quartz-lined tube furnace. The annealing of the alloys was done at a pressure of 10^{-3}torr under dynamic vacuum by means of a cryogenic sorption pump. This pump also condensed a large portion of water vapor in the quartz tube. Water vapor becomes one of the main gaseous constituents in high vacuum and is an oxidizing agent for Cu [35] and Si. Ampule shaped end section of the quartz tube, separated from the main body with a constriction, held fine Cu powder to react with and further reduce the concentration of the residual oxidizing agents.

Some alloys were subjected to cold rolling; however, this procedure was discontinued since it produced cracks in hard alloys. In all, 118 alloys were prepared to cover terminal solid solution and the adjacent two-phase region at Cu-Au-rich end of the diagram.

Following the annealing, part of the alloy slug was filed into a powder and the rest imbedded in plastic resin for micrographic analysis. The powder was sieved through a #325 mesh and annealed in dry N_2 atmosphere at 125°C to remove mechanical strain. Capillary quartz tubes, 0.2 or 0.3 mm in diameter filled with the powder were loaded into 114.6 mm diameter Debye-Scherrer cameras. X-ray diffraction pattern of the powder was then obtained using Ni filtered CuKα radiation from a Norelco unit. Lattice parameter data were obtained from the diffraction pattern by making a least square fit of a straight line to the experimental data versus Nelson-Riley extrapolation function.

The preparation of the alloys for micrographic analysis was done by polishing the alloys in Al_2O_3 powder on a fine felt cloth. The final polishing step was done in 0.05μ alumina; the following etch was used to stain the alloys by lightly swabbing it on the surface:

$$1 \text{ ppV } H_2O + 1 \text{ ppV } NH_4OH + 1 \text{ ppV } (10\%)\ H_2O_2$$

The analysis was performed with an optical microscope at 500X and 1250X magnification, using color and polarizing filters to enhance the color contrast of the phases. Percentage volume occupied by the phases was analyzed by measuring the length of the intercept of areas on multiple random straight lines drawn on micrographs of the polished alloy surfaces.

B. Results

The boundary of the terminal solid solution was determined over most of the Cu-Au end of the phase diagram (Fig. 13). Si solubility was measurable but below the estimates obtained by interpolating the solubilities in Cu-Si and Au-Si binary systems. The compositions of the alloys that determine the boundary are given in Table 1. The terminal solid solution, which had FCC space lattice, was found to be in equilibrium with a cubic phase, which was identified as the cubic γ-phase of the Cu-Si system possibly incorporating some Au atoms.

Powder X-ray diffraction pattern analysis indicated that the alloys contained γ-phase at Si concentrations above 4-5 atomic percent. This phase was identified by comparing the powder pattern with that reported in the literature [36]. The lattice parameter of this phase was found to be 6.322$\mathring{A}$, about 1.5% larger than the value reported for this phase in the Cu-Si binary phase. The increase in lattice parameter may be due to substitution of Au atoms for Cu in the γ-phase.

The Au-Cu-Si ternary phase was found to have FCC space lattice at all compositions. The lattice parameter of the alloys at the phase boundary fell within uncertainty of lattice parameter data reported for Cu-Au binary alloys.

The γ-phase was characterized by its high hardness, brittleness, and pale-gray color in contrast to the more ductile and light-bronze-yellow colored ternary phase, in micrographic analysis. These observations were also in essential agreement with the literature [37-39]. The γ-phase was observed to form 2-10μ spherodized crystallites imbedded in the ternary alloy.

Fig. 13

Phase diagram of Cu-Au-Si at Cu-Au rich end, at 349^{o}C. Only the alloys closest to the boundary are shown. The phase boundary is drawn between the open circles representing one-phase region and open squares representing two-phase region.

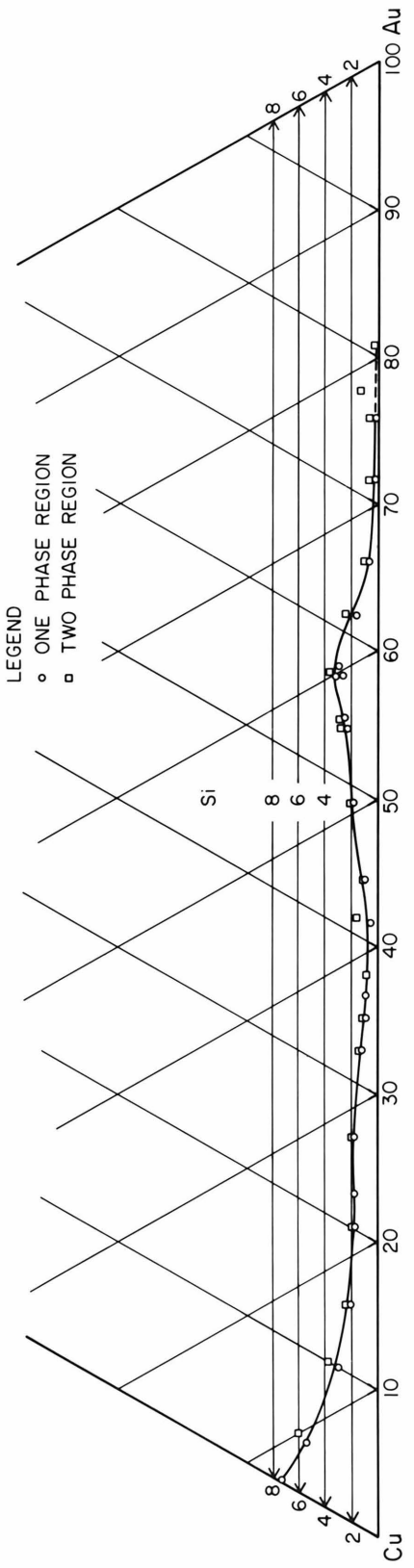
LEGEND
ONE PHASE REGION
TWO PHASE REGION
Si
8
6
4
Cu
2
4
6
8
10
20
30
40
50
60
70
80
90
100 Au

Electron microprobe analysis of a limited number of alloys confirmed the homogeneity of the individual phases.

Analysis of the alloys with low Si concentrations in the two-phase region indicated that micrographic analysis was more sensitive than powder pattern analysis. Hence the boundary has been determined by disappearing phase method mainly by relying on micrographic data: Alloys were prepared with decreasing Si concentration until the second phase could not be observed. The uncertainty in the location of the boundary is less than ∓ 0.2 atomic percent.

A different analysis of the alloys indicated the location of the boundary, with larger uncertainty, confirming however, the results obtained by the previously mentioned method: The volume percentage of the second phase (γ) plotted versus Si concentration for alloys in the two-phase region was extrapolated to Si concentrations at which γ-phase would disappear. The extrapolated concentration of the alloy fell at or within 0.5 atomic percent of the boundary determined by micrographic analysis.

C. Discussion

The length of the annealing time was considered to be adequate for the system to reach equilibrium. The mobility of Cu atoms in the alloys at this temperature was large compared to average metal diffusivities as indicated by diffusion studies in Cu-Au alloys [40]. Similarly, previous investigation [41] of the peritectic dissociation of the K-phase into the α and γ-phases in the Cu-Si binary system had indicated that this transformation occurs most rapidly in the temperature interval

TABLE 1

THE COMPOSITION OF THE ALLOYS AT TERNARY SOLID SOLUTION PHASE BOUNDARY

Si	Au	Cu
7.4	0	92.6
4.9	3.9	91.2
3.4	10.1	86.5
2.8	14.2	83.1
1.9	19.8	78.3
1.7	22.6	75.7
1.7	26.2	72.1
1.5	32.1	66.4
1.1	34.4	64.5
0.9	36.4	62.7
0.9	37.5	61.6
1.1	41.2	57.5
1.3	43.8	54.9
1.8	44.9	53.3
2.0	53.2	44.8
2.6	53.6	43.8
3.1	57.5	39.4
2.2	61.6	36.2
0.4	71.8	27.6
0.2	75.3	24.5

300-450°C, and that it reaches completion at time intervals comparable to our annealing times [37]. This peritectic dissociation is the most sluggish transformation in this system. Thus kinetic data from two of the binary systems suggested that ample time was allowed for the ternary system to reach equilibrium. The decrease of Si concentration at the boundary of the ternary phase with addition of Au can be explained with the expected change in chemical-physical properties of Cu-Au alloys from those of pure Cu to those of pure Au as relative concentrations of the latter in the binary alloys change. Similar behavior is observed in Au-Cu-Ge, Au-Cu-In [42] where solubilities of Ge or In in Cu-Au decreases as Au concentration of the ternary alloy increases, and Au-Ag-Sn where boundary of ternary phase changes linearly in accordance with the linear interpolation of the binary solubilities in Au-Sn and Ag-Sn systems.

Investigation of Au-Si-Ag system [43] which is analogous to the presently studied Au-Si-Cu indicated that there is a limited ternary solid solution. The Si concentration, however, was not reported. The deviation from a monotonic decrease in Si concentration of the ternary phase boundary between 45-65% Au concentration coincides with the range of solid solutions in binary Cu-Au alloys where ordering is observed.

Diffusivities, hence kinetics of phase transformation are expected to be more sluggish in an ordered solid solution on account of the higher activation energy for diffusion [40]. Therefore, it is possible that annealing time for the alloys in this compositional range was not long enough for the

equilibrium to be established. However, careful examination of the powder pattern did not reveal formation of the ordered solid solution.

C. Conclusion

The phase boundary of the binary solid solution in the Cu-Au-Si system has been determined at $349 \mp 1^{o}C$. The analysis was done by the disappearing phase method using powder X-ray diffraction and micrographic analysis. The ternary solid solution was observed to be in equilibrium with a cubic phase richer in Si, identified as the γ-phase of the Cu-Si system possibly incorporating Au atoms.

The phase boundary was poorer in Si concentration than the estimates based on linear interpolation of binary solubilities of Si in Cu and in Au. The Si concentration of the alloys at the boundary decreased upon addition of Au monotonically up to 40% Au, then showed an increase which peaked at $\sim$56% Au.

REFERENCES

1. M. Hansen, Constitution of Binary Alloys (McGraw Hill Co., N. Y., 1958), p. 232.
2. C. di Capua, Rend. Nazl. Lincei 29, 111 (1920).
3. E. G. Heath, J. Elect. Control 11, 13 (1961).
4. W. Gerlach, B. Goel, Sol. St. Elect. 10, 589 (1967).
5. T. A. Trumbore, Bell Systems Tech. J. 39, 205 (1960).
6. W. Klement, R. H. Willens, D. Duwez, Nature 187, 869 (1960).
7. T. R. Anantharaman et al., Nature 210, 1040 (1966).
8. P. Predechi, B. C. Giessen, N. J. Grant, Trans. AIME 233, 1438 (1965).
9. E. Philofsky et al., J. Electrochem. Soc. 119, 527 (1972).
10. G. A. Andersen et al., Mat. Sci. Eng. 7, 83 (1971).
11. H. S. Chen, D. Turnbull, J. Appl. Phys. 38, 3646 (1967).
12. R. C. Krutenat, J. K. Tien, D. E. Fernwalt, Mat. Trans. 2, 1479 (1971).
13. T. Narusawa, S. Komiya, A. Hiraki, Appl. Phys. Lett. 20, 272 (1972).
14. V. A. Filanenko, Russ. J. Phys. Chem. 43, 874 (1969).
15. M. W. Ozelton et al., Rev. Int. Homtes Temp. Refract. 4, 109 (1967).
16. H. S. Chen, D. Turnbull, Appl. Phys. Lett. 10, 284 (1967).
17. H. M. Breitling, R. E. Hummel, J. Phys. Chem. Solids 33, 845 (1972).
18. A. Shumka, R. Piety, 13th Ann. Rel. Phys. Symp., Las Vegas (1975).
19. H. Day, A. Christan, D. J. Bressman, to be published.
20. A. Hiraki, M. A. Nicolet, J. W. Mayer, Appl. Phys. Lett. 18, 178 (1971).
21. A. Hiraki, E. Lugujjo, J. Vac. Sci. & Tech. 9, 155 (1971).

22. A. Hiraki, E. Lugujjo, J. W. Mayer, J. Appl. Phys. 43, 3643 (1972).

23. H. Sankur, J. O. McCaldin, J. Electrochem. Soc. 122, 565 (1975).

24. E. R. Jeble, E. B. Gebert, J. Chem. Phys. 1, 753 (1933).

25. M. Hansen, Constitution of Binary Alloys (McGraw Hill Co., N.Y., 1958), p. 629.

26. Same as Ref. 25, p. 198.

27. S. S. Lau, R. C. Sun, Thin Solid Films 10, 273 (1972).

28. V. S. Sotnikov, A. S. Belanovski, Russ. J. Phys. Chem. 34, 1001 (1960).

29. W. Kern, RCA Review 31, 234 (1970).

30. G. B. Larrabee et al., J. Electrochem. Soc. 114, 867 (1967).

31. J. Van der Meulen, J. Electrochem. Soc. 119, 530 (1972).

32. L. D. Locher, C. D. Capio, J. Appl. Phys. 44, 4366 (1973).

33. D. Gupta, K. W. Asai, Thin Solid Films 22, 121 (1974).

34. A. Yanagisawa, M. Namba, Japan. J. Appl. Phys. 12, 748 (1973).

35. R. Vogel, W. Pocher, Z. Metallkunde 21, 333 (1929).

36. S. Arrhenius, A. Westgren, Z. Phys. Chem. (B) 14, 66 (1931).

37. W. R. Hibbard, G. H. Eichelman, W. P. Saunders, Trans. AIME 180, 92 (1949).

38. C. S. Smith, Trans. AIME 83, 414 (1929).

39. A.G.H. Andersen, Trans. AIME 137, 334 (1940).

40. M. Khubaib, K. P. Gupta, Scripta Metall. 4, 605 (1970).

41. A. D. Hopkins, J. Inst. Met. 82, 1508 (1953).

42. H. W. Krug, T. B. Massolski, L. L. Isaacs, Acta Metall. 11, 1355 (1963).

43. V. V. Kuprina, Russ. J. Inorganic Chem. 7, 833 (1962).